

A MICROFLUIDIC INVESTIGATION OF CALCIUM OXALATE
CRYSTALLIZATION

By

JINNIE ANSTICE

A thesis submitted to the

Graduate School-Camden

Rutgers, The State University of New Jersey

In partial fulfillment of the requirements

For the degree of Master of Science

Graduate Program in Chemistry

Written under the direction of

Dr. George Kumi

And approved by

Dr. George Kumi

Dr. Alex J. Roche

Dr. Hao Zhu

Camden, New Jersey

May 2018

THESIS ABSTRACT

A microfluidic investigation of calcium oxalate crystallization

By JINNIE ANSTICE

Thesis Director:
Dr. George Kumi

Calcium oxalate crystallization is widely studied due to the prevalence of this substance in various biomineralization processes, especially the formation of kidney stones. Bulk crystallization studies are a common and popular method for investigating calcium oxalate in particular. Crystallization studies using microfluidic platforms are becoming more popular because of the simplicity of use, cost effectiveness and enhanced control of system variables that these systems offer. Microfluidic systems using a two-input, one-output design results in crystallization at the entrance of the microchannel. This could lead to clogging of the device, and clogging makes it difficult to study crystallization over long lengths of time using these devices. In this study a three-input, three-output microfluidic channel system was designed and a protocol was established that minimized bubble occurrence and synthesized calcium oxalate crystals within the device; crystals were analyzed ex-situ. Equimolar input salt concentrations (CaCl_2 , $\text{K}_2\text{C}_2\text{O}_4$) of 20, 40 and 60 mM were used in these experiments. Evidence of crystallization within the device was a line forming in the center channel that grew (i.e., darkened) over time. As the concentration of input salt solution increased, the time that it took for the line to be visible decreased but the length and darkness of the line increased. In order to re-use devices hydrochloric acid was tested as a cleaning solvent, and it proved to be an

appropriate solvent that did not alter the crystallization process. Experiments in which sodium polyacrylate (a common additive in calcium oxalate crystallization experiments) was added to the system showed that the additive inhibited the growth of crystals formed within the microfluidic device. Analysis of collected crystals was done by optical and scanning electron microscopy.

Dedication

I would like to dedicate this thesis to my amazing husband Shane. Without his support, encouragement and sacrifice I could not have reached this goal. For ten years he has been picking me up when I fall down, wiping my tears, brushing me off and pushing me to get back on track. Thank you for all that you do.

I also dedicate this work to my children. They have watched me spend many hours in front of the computer, reading a textbook or practicing flashcards. They have tolerated me working at their extracurricular activities and have understood the commitment necessary to achieve this goal. I wish them all the best and don't ever give up on your dreams.

Finally, I dedicate this thesis to my family and friends especially my brother, Kevin. Thank you for not letting me fall. To my firehouse family, my campground family and all of my wonderful friends thank you for your understanding and patience throughout this process.

Acknowledgements

Rutgers-Camden, specifically the science department, has been a second home to me for the last ten years. I came to Rutgers as a non-traditional student with high hopes of achieving my goals. Rutgers- Camden was a welcoming and supportive environment especially for students in complicated situations or with family obligations. It was wonderful to have access to professors, tutors, and multiple programs that assist students, especially non-traditional students.

First, I would like to thank Dr. Alex J. Roche, who tolerated my endless office visits while trying to wrap my head around organic chemistry. I am also thankful he accepted the task of being on my thesis committee. Lastly, I want to thank Dr. Roche for recommending me as a work study student for Dr. Arbuckle-Keil which opened up numerous opportunities for me.

Dr. Arbuckle-Keil and I had an instant connection almost a decade ago. I wanted to learn, and she wanted to teach. Together we have tackled many things over the years. Thank you for believing in me and pushing me to be the best that I can be not only as a student and colleague but as a person. It is always a joy to see her in the lab, especially when she is determined to fix an instrument. Dr. Arbuckle-Keil is a role model and strong advocate for women in science. Thank you for providing me with the many opportunities that I had at Rutgers. I look forward to our talks after this chapter of my life has closed.

Ms. Mary Craig is another woman that I have had the pleasure of working with throughout my time at Rutgers-Camden. Ms. Craig has been an integral part of this process and my success as a student, colleague, educator, parent, and spouse. She always

knows what to say no matter what the situation. I would not have made it without relying upon her simple but meaningful words of wisdom.

I would also like to thank Dr. Zhu for being on my committee. Thank you for making me see bigger connections. Thank you to Sarah Belh and Todd Grover for the endless hours of entertainment in the lab. Thank you to Peter Fazzino and Janet Caruso for their help in the office (and Janet for sharing my birthday).

My deepest thanks go to Dr. Kumi for taking me into his group and committing to be my advisor. It is always such a pleasure to see Dr. Kumi interact with his students, both undergraduate and graduate. He has a genuine interest in seeing his students succeed. I appreciate your talent to explain things and value your wisdom and expertise and an advisor and an educator. Thank you for your patience and understanding throughout this long process.

Table of Contents

Title	i
Abstract	ii
Dedication	iv
Acknowledgements	v
Table of Contents	vii
List of Figures	x
List of Tables	xv
Chapter 1: Introduction	1
1.A. Urolithiasis	1
1.B. Calcium Oxalate Contribution	2
1.C. Microfluidics	5
1.D. Research Objective	10
Chapter 2: Experimental Method and Materials	12
2.A. Microfluidic Device Fabrication	12
2.A.1. Glass Substrate Preparation	12
2.A.2. Master Structure Fabrication	13
2.A.3. Replica Molding	17
2.B. Device Operation	18
2.C. Establishing the Crystallization Protocol	19

2.C.1.Bubble Reduction.....	19
2.C.2. Device Flow Characterization	21
2.C.3. CaOx Crystallization	22
2.C.4. Crystal Collection and Analysis.....	23
2.C.5. Establishing re-usability of device	24
2.C.6. Additives (addition of NaPA)	24
Chapter 3: Results and Discussion	26
3.A. CaOx crystallization and analysis	26
3.A.1. Establishing reproducibility using the same master structure.	28
3.A.2. Establishing reproducibility using different master structures.	31
3.A.2.a. 60 mM concentration inputs.....	32
3.A.2.b. 40 mM concentration inputs	34
3.A.2.c. 20 mM concentration inputs.....	36
3.A.3. Summary of results	38
3.B. Concentration Comparisons	38
3.B.1. Summary of results	38
3.C. Use of HCl as a solvent.....	40
3.C.1.a. Device 2 comparisons before and after HCl	41
3.C.1.b. Device 3 comparisons before and after HCl.....	43
3.C.1.c. Device 4 comparisons before and after HCl	45

3.C.1.d. Device 5 comparisons before and after HCl.....	47
3.C.2. Summary of results	48
3.D. Effects of additive on CaOx crystallization.....	49
3.D.1.a. 1 mM NaPA	49
3.D.1.b. 5 mM NaPA.....	50
3.D.1.c. 10 mM NaPA.....	51
3.D.2. Summary of results	52
Chapter 4: Future Work	53
References	58
Appendix	62
A.Master structure fabrication.....	61
B.Pump start up traits	61

List of Figures

Figure 1. Commonly occurring calcium oxalate shapes (obtained from Reference 8)	4
Figure 2. Model of three-stream microfluidic device to be used in study	11
Figure 3. (a) Glass functionalization reaction (b) APMS structure	13
Figure 4. Chemical structures of (a) TPO-L (b) SR368 and (c) SR399	14
Figure 5. (a) Schematic of set up for making master structure, (b) image of actual transparency mask, and (c) the chemical structure of tridecafluoro-1,1,2,2-tetrahydroctyl dimethylchlorosilane	15
Figure 6. Completed master structure	16
Figure 7. Cracked master structure	17
Figure 8. (a) PDMS mold with inserted channel tubing. (b) Optical image of cross – section of microchannel (~300 μm high x 15000 μm long x 800 μm wide)	18
Figure 9. (a) Bubbles in the device that have altered fluid flow profile.(b) Schematic of experimental set up and (c) actual experimental set up	20
Figure 10. (a) Image of device prior to any dye fluid flow and (b) laminar flow profile of dye solution. Flow rates of the red and green are 20 $\mu\text{L}/\text{min}$ and center 50 $\mu\text{L}/\text{min}$. Arrow indicates direction of fluid flow	22
Figure 11. Image of “salt line” (CaOx crystal line) forming in the center channel of device. Arrow points to salt line forming in center channel	23
Figure 12. Damaged master structure after successive molds	28

Figure 13. Damaged master structure after successive molds	28
Figure 14. (I) The initial flow profiles of devices 1A, 1B and 1C are relatively similar. (II) After introducing the salts into the device, the first sign of CaOx formation in the device was 5 min. for device 1A, 6 min. for device 1B, and 7 min. for device 1C. Arrows point to where salt line is in the channel. The dashed lines depict the channel walls	29
Figure 15. (I) The line continued to grow and darken over time. At ~12 min., the line was similar in length and darkness for all three devices. (II) The final profile check for all three devices suggests laminar flow remained throughout crystallization in the device. Arrows indicate where crystallization is evident in the channel the dashed lines depict the channel walls	30
Figure 16. Microscopic images of crystal collection results. Representative images were chosen from device 1A, 1B, and 1C collections. Scale bars of optical images are 35 μ m	31
Figure 17. (a) 60 mM input concentration comparisons. (I) Salt line appearance: 4 min.(2A), 5 min.(3A), 5 min.(4A), and 7 min.(5A). (II) Salt line growth: 7 min.(2A), 13 min.(3A), 6 min.(4A), and 9 min.(5A). (III) Salt line growth: 10min.(2A), 16 min.(3A), 18 min.(4A), and 11 min.(5A). Arrows indicate where crystallization is evident in the channel. (b) Representative collection of 60 mM input concentration CaOx crystals scale bars of optical images are 35 μ m	33
Figure 18. (a) 40 mM input concentration comparisons. (I) Salt line appearance: 7 min.(2B), 7 min.(3B), 16 min.(4B), and 7 min.(5B). (II) Salt line growth: 21 min.(2B), 26 min.(3B), 28 min.(4B), and 26 min.(5B). (III) Salt line growth: 55 min.(2B), 41 min.(3B),	

49 min.(4B), and 46min.(5B). (b) Representative collection of 40 mM input concentration CaOx crystals scale bars of optical images are 35 μm	35
Figure 19. (a) 20 mM input concentration (I) Salt line appearance at 30 min. (2C) and 20 min. (3C). (II) Salt line at 50 min. (2C,3C). (b) Optical images of representative collection of 20 mM input concentration CaOx crystals. Scale bars of optical images are 35 μm . (c) SEM images of representative collection of 20 mM input concentration CaOx crystals. Scale bars of SEM images are 10 μm	37
Figure 20. Comparison of salt line darkness and growth over time. (I) Device 2A (20 mM), 2B (40 mM), 2C (60 mM). (II) Device 3A (20 mM), 3B (40 mM), 3C (60 mM). Vertical arrows indicate the end of salt line growth in center channel. Horizontal arrows indicate fluid flow direction	39
Figure 21. Comparison of salt line darkness and growth over time. (I) Device 4A (20 mM), 4B (40 mM), 4C (60 mM). (II) Device 5A (20 mM), 5B (40 mM), 5C (60 mM). Vertical arrows indicate the end of salt line growth in center channel. Horizontal arrows indicate fluid flow direction	40
Figure 22. (a) Microscopic optical image of Device 3B before HCl flush. Device had crystals left in the channel after experiment and water flush. (b) Device 3B after HCl flush. Crystals appear to be removed completely. This image is representative of the same results for all other devices	41
Figure 23. Initial (a, b) and final (c, d) appearance of salt line for the “before HCl” and “after HCl” experiments using Device 2A	42

Figure 24. Initial (a, b) and final (c, d) appearance of salt line for the “before HCl” and “after HCl” experiments using devices made from master structure 2. Images for (I) Device 2B, (II) Device 2C	43
Figure 25. Initial (a,b) and final (c,d) appearance of salt line for the “before HCl” and “after HCl” experiments using Device 3A	44
Figure 26. Initial (a,b) and final (c,d) appearance of salt line for the “before HCl” and “after HCl” experiments using Device 3B	45
Figure 27. Initial and final appearance of salt line for the “before HCl” and “after HCl” experiments using devices made from master structure 4. Images for (I) Device 4A, (II) Device 4B and (III) Device 4C	46
Figure 28. Initial (a,b) and final (c,d) appearance of salt line for the “before HCl” and “after HCl” experiments using Device 5A	47
Figure 29. Initial (a,b) and final (c,d) appearance of salt line for the “before HCl” and “after HCl” experiments using devices made from master structure 5. Images for (I) Device 5B, (II) Device 5C	48
Figure 30. (I) Salt line appeared at 5 min. for 60 mM input concentration with 1 mM NaPA (6P1). (II) Line continued to grow over time but not as much as without additive (III) optical and (IV) SEM images of CaOx formed with addition of 1 mM NaPA. Optical images scale bar is 10 μ m SEM scale bar is 5 μ m	50
Figure 31. (I) Salt line appeared at 8 min. for 60 mM input concentration with 5 mM NaPA (6P5). (II) Salt line for 5 mM NaPA additive not as dark or long as the other trials	51

Figure 32. A salt line was not evident in the channel after 20 min. using the 10 mM NaPA additive (6P10)	51
Figure 33. (a) 1 mM, (b) 5 mM, (c) and 10 mM NaPA concentration comparison after 20 min	52
Figure 34. (a) Image of crystal line breaking into pieces. (b) Schematic of cross-section current microchannel design and crystals forming near the surface. (c) Schematic of future microchannel design	52
Figure 35. Chemical structures of polyglutamic acid monomer (a) and polyaspartic acid monomer (b)	57

List of Tables

Table 1. List of definitions and buzzwords relating to “lab on chip” technology. Table adapted from Reference 23	6
Table 2. Summary of Mark et al. review of microfluidic platforms	9
Table 3. Labels used for devices discussed in this study specifying the master structure and concentration input used	27

CHAPTER 1: Introduction

1.A. Urolithiasis

Biom mineralization is the process by which biological organisms form minerals or crystalline structures. Stone formation, or lithiasis, is a common consequence of biom mineralization and can occur in several different organs. Examples of stone formation include: kidney lithiasis (nephrolithiasis), ureter (ureterolithiasis), or bladder (cystolithiasis). Urolithiasis refers to a stone formed anywhere in the urinary system but is often referred to as “kidney stones”. Kidney stones affect 1 in 11 people in the United States.¹ Statistical studies have shown that men have a higher prevalence of developing a stone over women.^{1,2} Those with obesity and diabetes were associated more closely to the disease than normal weight individuals. Also, Hispanic and Black individuals were at less risk than White individuals. Based on this information it is suspected that diet and lifestyle contribute to the changing epidemiology of kidney stones.^{1,2}

Not only can this disease be extremely painful and debilitating during an episode, it can cause a financial strain on the individual. Most reported cases of kidney stones are from the working-age population.¹ An episode of a kidney stone can cause hospitalization, surgery, loss of wages and pharmaceutical costs. However, these consequences do not fall solely on the individual with this disease. Although the diagnosis and treatment of urolithiasis has decreased slightly over the years, about 1.3 million emergency department visits were recorded in the year 2009 with about 20% of these cases resulting in hospitalization. Emergency department visits for kidney stone disease increased 20% between 2005 and 2009.^{3,4} The projected cost of urolithiasis diagnosis and treatment is \$1.24 billion dollars by the year 2030.⁵ Due to the evident

increase in stone disease and its economic impact on our society it is imperative to study and understand the disease.

1.B. Calcium Oxalate Contribution

Common stone-forming salts include, calcium oxalate, uric acid, cysteine and struvite. Renal stones, stones occurring in the kidney and lower urinary tract, are comprised of many components. The main inorganic component in most renal stones is calcium oxalate (CaOx) which can contribute up to 80% of a stone structure.⁶ The remaining portion of the stone is an organic matrix of proteins, lipids, and carbohydrates.⁷ Oxalate can either be ingested (endogenous oxalate) or produced (exogenous oxalate) in the body. The body will secrete Ca^{2+} ions into the urine, or tubular fluid, to conserve water.⁸ Human urine is supersaturated with CaOx, and CaOx crystals can be found in either stone formers or non-stone formers.⁹ Possible causes and mechanisms of kidney stone formation are not fully understood but widely studied. Formation of renal stones could be the result of many biological consequences including, but not limited to: a genetic mutation that alters metabolism and homeostasis, renal adhesion or failure of inhibitory proteins.^{7,10-14}

There are two events contributing to crystal formation; nucleation and growth/aggregation. Nucleation (crystallization from solution) occurs when calcium oxalate saturation exceeds the limit of metastability.⁹ The initial event of crystal formation can occur either homogeneously or heterogeneously. Homogeneous nucleation occurs when supersaturation results in the bonding of molecules into a lattice structure. Heterogeneous nucleation is when the precipitate binds to some sort of substrate.

Heterogeneous crystal formation is more common in complex mixtures such as urine.^{9,15} Aggregation, a form of crystal growth of the crystal, is the result of the attachment of several nuclei to form a polycrystalline structure. The crystal aggregation process dictates the overall shape of the crystal aggregate.

Several hydrates of the CaOx crystal can form, namely: calcium oxalate monohydrate (COM), calcium oxalate dihydrate (COD) and calcium oxalate trihydrate (COT) (Figure 1)¹⁰. COM ($\text{CaC}_2\text{O}_4 \cdot \text{H}_2\text{O}$), also known as whewellite, is the most stable CaOx hydrate at typical room temperatures and pressures. COT ($\text{CaC}_2\text{O}_4 \cdot 3\text{H}_2\text{O}$) is the least stable polymorph at the conditions previously mentioned.^{10,16,17} COM and COT crystals are formed in healthy patients as well as patients that suffer from stone disease. Several factors, including molar concentration of ions, order of addition of calcium and oxalate ions, presence of buffer, pH, stirring rate, and temperature determine the type of hydrate that forms.¹⁰ However, the monohydrate (COM) is the most common form found in the stone matrix and is frequently studied.

Nucleation and growth of a single crystal will not yield a crystal big enough to be lodged in the urinary system¹⁴. Therefore, it is a common belief that aggregation is the crucial step in the attachment of stones to renal tubules and epithelial cells. Many studies have been conducted on the effects of urinary constituent attachment to CaOx crystals. Certain urinary proteins may inhibit or promote the formation of specific CaOx forms.^{17–19} For example, osteopontin was shown to promote (COD) crystallization.²⁰ Citrate, another common urinary protein, inhibits growth and attachment of COM crystals.^{13,14} These protein-CaOx interactions could possibly depend on: the chemical structure of interacting groups, protein chain length, or spatial arrangement of the inhibiting species.




Figure 1. Commonly occurring calcium oxalate shapes (image obtained from Reference 8).

Studies using polyelectrolytes (e.g., polyacrylic acid (PAA), polyaspartic acid (PolyD), polyglutamic acid (PolyE)) have shown the tendency of certain additives to adhere to crystal faces and alter CaOx growth, shape, and attachment to renal tubules.²¹ These specific additives are thought to mimic urinary protein function. Anionic surfactants are polymeric additives reported to have the strongest CaOx growth inhibition effect.¹⁷ It has been shown that the biological surfactants can lower surface tension of the crystal face and therefore inhibit crystal growth. Common inhibitors typically have one or more carboxylate groups. The anionic carboxylate ion has a strong affinity for the positively charged Ca^{2+} . It is possible that certain hydrates of CaOx may be more likely to attach to renal tubules. Methods used in previously published CaOx crystallization

studies include: bulk crystallization, well-plates, and lipid monolayers.^{4,5,7,8,15,19,20} At the time of this work there were no microfluidic studies of CaOx crystallization. Acquiring insight into COM formation is essential to understanding stone formation and developing effective treatment.

1.C. Microfluidics

Microfluidics is the field of science and technology that involves the use of devices, with micrometer dimensions, to manipulate a fluidic environment. The benefits of microfluidic systems include: the ability to use small sample amounts, high sensitivity, high resolution, short analysis times, and control of concentration of molecules in space and time.²⁴ Several branches of science can benefit from microfluidic applications. By 2009 there had been almost 10,000 papers published on microfluidics and over 1000 USA patents recorded.²⁵ Microfluidic origins stem from its parent applications in analysis, biodefense, molecular biology and microelectronics.²⁴

Analytical techniques such as high-pressure liquid chromatography (HPLC) gas-phase chromatography (GPC) and capillary electrophoresis (CE) opened the door for development of other microscale methods that provide high sensitivity and resolution. A successfully miniaturized (GC) was developed in 1979, and in 1990 the first microfluidic HPLC device was published.²⁵ Then, in the 1990's, the US Department of Defense found it necessary to support a series of programs to design microfluidic, deployable detectors for chemical and biological threats.²⁴ This government support fueled microfluidic growth. Molecular biology required a high throughput, high sensitivity and high

resolution system, that microfluidics could offer, following the explosion of genomics and DNA sequencing.²⁴

Photolithographic techniques and microelectromechanical systems (MEMS) were very successful for microelectronics, where systems were typically made from silicon and glass. However, these materials were not conducive to fabricating a device targeted at biological samples.²⁴ Silicon and glass are thermally and chemically stable, and therefore geared toward more specialized systems.²⁴ The basis for ink-jet technology was established in the early 1950's when nanoliter and picoliter sized liquids were dispensed from a microfluidic device.²⁵ The microfluidic devices are also referred to as micro total analysis systems (μ TAS) or "lab on chip" systems. Over time several buzzwords have emerged referring to miniaturized systems. Table 1 provides a list of definitions relating to "lab on chip" technology.^{22,23}

μTAS (micro total analysis system)	An integrated analytic system that performs: sampling, sample pre-treatment, sample transport, chemical reactions, analytic separation, product isolation and detection.
'Lab-on-a-chip'	Widely used term for any miniaturized system, including microfluidic chips in addition to non-fluidic miniaturized systems such as sensors and arrays ("biochips").
Miniaturization	A technological fabrication that has the ability to be scaled-down or "miniaturized" without a difference in chemical quality.
Microfabrication	Fabrication processes that engineer flat surface substrates for example; photolithography, direct-write laser, etching, and film deposition.
Microsystem technology (MST) and micro-electromechanical systems (MEMS)	The fabrication of electronic or mechanical components on chips.
Microfluidics	Fabrication and research of liquid systems in chips consisting of micro-sized channels. Systems with channels of sub-micrometer size are referred to as 'nanofluidics'.

Table 1. List of definitions and buzzwords relating to "lab on chip" technology. Table adapted from Reference 23.

The most common methods for microfluidic device fabrication include: micromachining, replica molding, embossing, injection molding, and laser ablation.²⁷ Micromachining methods use glass or silicon as a material to fabricate a master structure from which disposable plastic devices can be replicated. Micromachining is not ideal due to the high cost of processing glass using harsh chemical techniques such as wet and dry etching, photolithography, and electron beam lithography. Silicon is expensive and opaque, and this opacity eliminates its use with optical detection methods.²⁴

Soft lithography is a replica molding technique using an elastomer, commonly polydimethylsiloxane (PDMS), to fabricate devices from a master structure (silicon, acrylate, etc.).^{24,27-31} PDMS is an optically transparent elastomer that is easy to use and cost effective. It has become the most common material used for early development in microfluidic research. The development of soft lithography has minimized prototyping from an average of one month (using silicon technology) to an average of two days.²⁴ The benefits of PDMS include, optical transparency, elastomeric nature, and compatibility with a variety of biological and cellular applications. However, due to its gas permeability it cannot be used for oxygen sensitive reactions, unless other preventative measures are taken. PDMS is mostly limited to aqueous solvents due to its incompatibility with many organic solvents.²⁷ Another type of replica molding, similar to soft lithography, involves the use of a thermoset polyester (TPE). Fabrication using a TPE molding differs from PDMS molding in that a TPE is not elastomeric and completely hardens when cured and it requires use of different interconnects. TPE is transparent, compatible with nonpolar solvents, and not gas permeable. The biggest difference between TPE and PDMS are the material properties.

Embossing fabrication consists of a thermoplastic material (that can be reshaped when heated near the glass transition temperature) and a silicon or metal stamp being pressed together and heated to form a mold. Embossing is not ideal for prototyping because of the time-consuming fabrication of the stamp. If access to a hydraulic press is available, this fabrication method is time and cost effective. Injection molding requires thermoplastic pellets be melted and injected under high pressure into a heated mold cavity. Master structure molds are produced similarly to methods used for embossing. This method is not commonly used in research laboratories because of the necessary equipment required. However, if the mold and master structure are of high quality, this is a precise large-volume replication method. Laser ablation uses a high-powered pulsed laser to remove unwanted sections of polymer which result in desired channels. The channels can be created either by a lithographic mask or by a direct write program. Laser ablation techniques are only used in specific studies. A major disadvantage of laser ablation is its cost and reduced throughput.²⁷

Microfluidic design and fabrication depend upon the system being studied and the materials being used. However, all devices consist of a component system including methods to: introduce reagents and samples, control fluidic movement within the chip, combine and mix fluids, and possibly detection or purification systems.²⁴ Mark, D. et al. address how to achieve a consistent fabrication and interfacing standard by establishing a microfluidic platform from the building blocks, or unit operations, of microfluidic laboratory protocols.²⁵ Table 2 summarizes their definitions of microfluidic platforms and can be used as a guide to determine a suitable platform for a specific application. The range of fabrication methods and component systems have evolved so much that

microfluidic applications can be used to start solving an array of research questions. A most common problem addressed is conditional screening (effects of pH, ionic strength, composition, solvents, concentration) of protein crystallization. Inorganic crystallization studies using microfluidic designs are growing in popularity in an attempt to explore the question of nucleation versus aggregation.^{32–34} Other applications include, separation of molecules, high throughput drug screening, and bio-analysis.^{24–26,29,31} Chemical synthesis in microfluidics continues to be a challenge mainly due to solvent compatibility. This study used a pressure driven laminar flow platform to investigate the effects of varying conditions on CaOx crystallization.

Definition of a microfluidic platform	A set of fluidic operations that can be combined with microfluidic systems for consistent miniaturization, integration, automation, and parallelization of (bio-) chemical processes.
Lateral flow tests	Lateral flow tests, also known as test strips (e.g. pregnancy test strip), and employ capillary forces and wettability of the porous substrate for liquid movement.
Linear actuated devices	Liquid movement is controlled by mechanical displacement such as by a plunger. This is limited to one dimensional linear flow systems.
Pressure driven laminar flow	Liquid transport is pressure driven by sources such as; syringes, pumps, pneumatics. Samples can be injected batch-wise or in continuous flow.
Microfluidic large scale integration	Chip-integrated micro-valves are coupled with a control channel. Pneumatic pressure applied to the control-channels opens or closes the micro-valves. Beneficial for use with multiple units on one chip.

Table 2. Summary of Mark et al. review of microfluidic platforms.

1.D. Research objective

Kidney stone disease has a global health and economic effect and is therefore worth investigating. There are many questions that can be addressed concerning the role of CaOx in the formation of kidney stones. When the details of CaOx crystallization are clearly understood the mechanisms that promote stone formation and attachment may also be better understood. New experimental and computational methods can bring major advancements in biomineralization studies. Microfluidics is a reliable, reproducible, fast, and cost-effective way of studying crystallization. Bulk crystallization studies can be affected by the presence of impurities. Many bulk crystallization studies have varying results and crystallization studies can take several hours, if not days, to complete. This is especially important when working with proteins because of the risk of denaturing over time. Many identical experiments can be done the same day with a microfluidic device. This allows a high throughput of results over a range of conditions which shortens experiment time. The flow system is dominated by laminar flow which is more controlled than traditional stirring or shaking. Microfluidic devices mimic the natural environment of some biomineralization processes that are diffusion-controlled.³³

The goal of this study was to fabricate a 3-input, 3-output microfluidic device and establish a protocol for reproducible investigations of CaOx crystallization. This was done by designing a three-stream microfluidic channel in which the Ca^{2+} and $\text{C}_2\text{O}_4^{2-}$ ions diffused into a center stream (Figure 2). Precipitated CaOx was collected into a saturated solution from the center stream. Once reproducible conditions were established the CaOx crystals formed were analyzed ex situ. Previous microfluidic crystallization studies utilized a two-channel design, which would result in crystallization at the interface of the

two CaOx component containing fluids.³³ Because of the potential for clogging, this type of design does not support a lengthy experimental time that allows for changing of several variables during the experiment. In this study, CaOx structural properties (i.e., habit and form) will be characterized by optical microscopy and scanning electron microscopy (SEM). Specific additives will be added into the diffusion stream (the center stream) to observe the effect of these additives on the crystallization process.

Determining the conditions specific to producing COM and COD formation in a microfluidic environment is an additional goal of this study. This work will impact future kidney stone and crystallization studies by providing a reliable and reproducible system for future studies on the crystallization of various inorganic crystals.

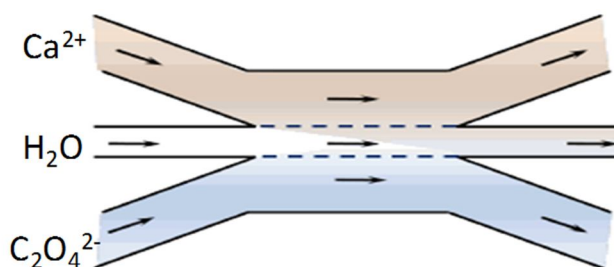


Figure 2. Model of three-stream microfluidic device to be used in study.

CHAPTER 2: Experimental Methods and Materials

2.A. Microfluidic Device Fabrication

2.A.1. Glass Substrate Preparation

Pre-cleaned glass microscope slides were used as substrates for the resin master structures. Using a process based on a previously reported technique, these glass slides were acrylate-functionalized to facilitate chemical bonding of the acrylate resin master structure.³⁵ In this process, glass slides were cleaned by sequentially submerging them into isopropyl alcohol (Sigma Aldrich), acetone (Sigma Aldrich), and distilled water for ~20 seconds each. This cleaning process is used to remove any macroscopic surface impurities, for example, dust particles. Cleaned slides were placed into slide rack (Wash-N-Dry Slide Rack, Electron Microscopy Services) and dried in an oven (Quincy Lab Model 10 Lab Oven) set at ~90°C for one hour.

Dried slides were then oxygen plasma-cleaned (Model PDC-32G Harrick Plasma coupled with a Harrick Plasma PDC-FMG pressure monitor) to remove surface residue and to produce a hydroxylated, hydrophilic surface. Oxygen plasma-cleaning was conducted at ~600 mTorr O₂ for 2-3 minutes. After plasma-cleaning, slides were immediately submerged into a 3-acryloxypropyltrimethoxysilane (APMS) solution for ~24 hours to functionalize glass (Figure 3). The APMS solution was a volume mixture of 93% ethanol, 5% water and 2% APMS. From this solution, the functionalized glass was then submerged in ethanol (Sigma Aldrich) for two hours, to remove any un-bonded APMS, and then oven dried at 90°C for one hour.

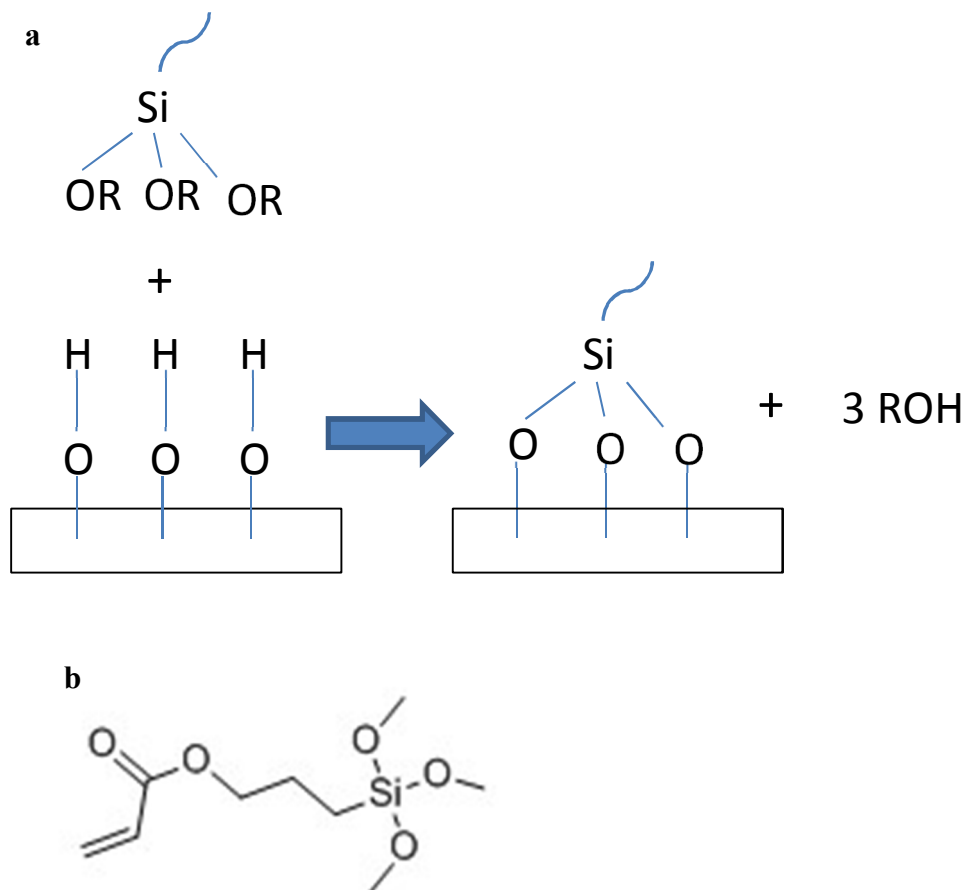


Figure 3. (a) Glass functionalization reaction (b) APMS structure.

2.A.2. Master Structure Fabrication

The master structure for the microfluidic device was made from a mixture of two acrylate resins, namely: tris (2-hydroxy ethyl) isocyanurate triacrylate (SR368, Sartomer) and dipentaerythritol pentaacrylate (SR399, Sartomer). The photoinitiator used in this acrylate resin was ethyl (2, 4, 6-trimethylbenzoyl) phenylphosphine. (TPO-L, BASF) (Figure 4). In this mixture, the concentration of the two acrylate resins was ~47.5 wt% while the photoinitiator concentration was ~5 wt%. The SR368 solidifies over time, therefore, it was heated for ~20 minutes at 100°C before mixing. The container for

mixing the resin (Supelco, 40mL Clear Vial, Screw Top) was wrapped in aluminum foil to prevent exposure to any ambient ultra-violet (UV) light which may initiate the polymerization. To ensure homogeneity in the resin formulation, this resin was mixed (Labnet Mini Labroller™) for ~24 hours.

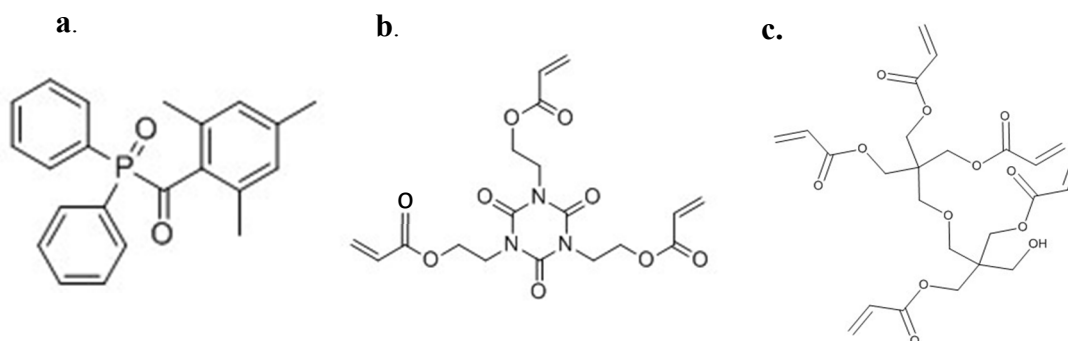


Figure 4. Chemical structures of (a) TPO-L (b) SR368 and (c) SR399.

Master structures were fabricated using standard photolithographic methods, and a computer aided design (CAD) program was used to create a transparency mask (Figure 5b).^{24,36} Four pieces of scotch tape were placed on both sides of the functionalized glass substrate to control the thickness of the master structure (~0.232 mm). To create a thin resin film, a few drops of the acrylate resin formulation (described in the preceding paragraph) were carefully placed on the functionalized slide. Then, this resin was covered with a fluorocarbon-coated (tridecafluoro-1,1,2,2,-tetrahydrooctyl dimethylchlorosilane) glass slide. The fluorocarbon-coated slides were prepared by (1) cleaning glass slides in the same manner as the cleaning process described in the preceding section, and (2) then vapor-depositing with a fluorocarbon onto these slides. To carry out this vapor deposition, slides were placed in a desiccator containing a watch glass with a few drops

of the fluorocarbon. The desiccator was evacuated using an aspirator (~2 minutes) and then the desiccator valve was closed for about 60 minutes. This process functionalized the glass substrates with a fluorocarbon which markedly reduces resin adhesion of acrylate to the slides.

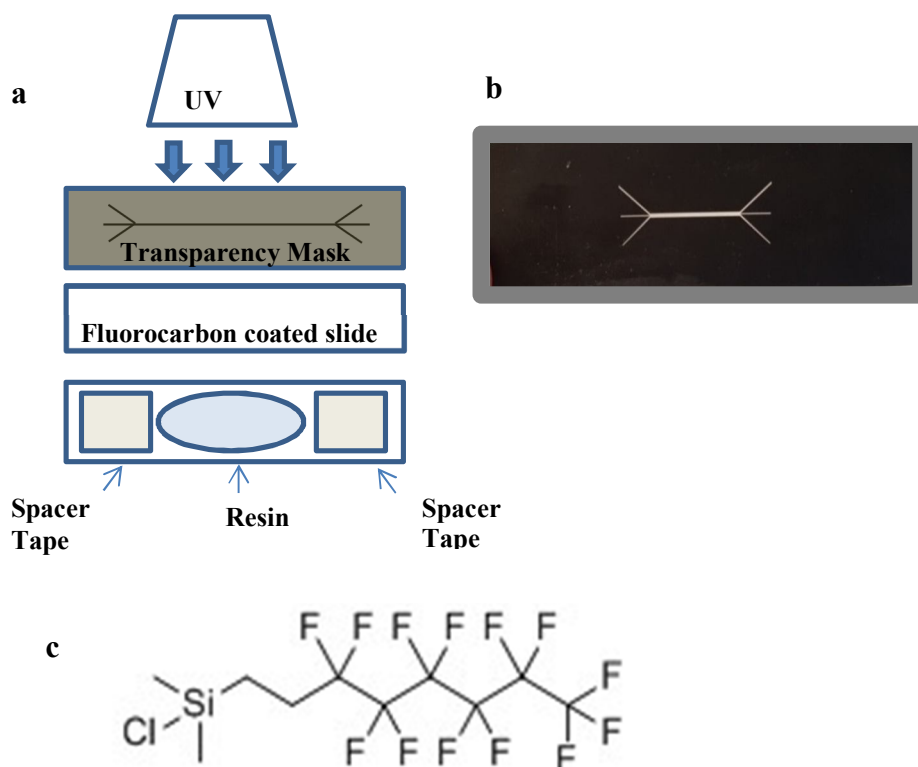


Figure 5. (a) Schematic of set up for making master structure, (b) image of actual transparency mask, and (c) the chemical structure of tridecafluoro-1,1,2,2-tetrahydrooctyl dimethylchlorosilane.

The aforementioned photomask was placed on top of the fluorocarbon-coated slide, and the entire assembly was placed under UV light (Blak-Ray B-100A, UVP) for ~90 seconds (Figure 5a). To minimize reflectance, which caused polymerization in undesired areas, the assembly was bordered with black paper. The UV light initiates

polymerization within the acrylate resin and at the interface of this resin with the functionalized slide. After removing the mask and fluorocarbon-coated slide, the acrylate-functionalized slide with resin film was then developed in acetone. Acetone development selectively dissolves any un-polymerized resin, leaving the polymerized regions of the resin on the glass slide (Figure 6).

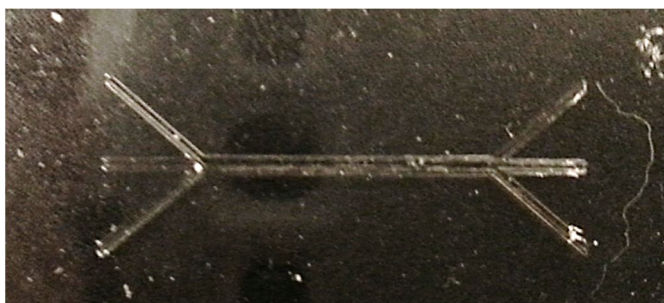


Figure 6. Completed master structure.

Two different acetone washes were used. The resin was dissolved in one acetone wash for ~60 seconds and then in another separate wash for the same amount of time. This “double washing” method proved to be the best at removing the leftover resin. The master structure was heated ($\sim 60^{\circ}\text{C}$, ~ 12 hours) to remove some of the remaining photoinitiator. The master structure was very sensitive to temperature changes. Heating at too high of a temperature caused cracking of the resin (Figure 7). However, insufficient heating of the master structure prevented cross-linking of the elastomeric polymer (i.e., the PDMS) used for replica molding at the master structure interface. Indeed, separate experiments show that the photoinitiator interferes with this cross-linking process (See Appendix). After heating, the resulting master structure was fluorocarbon-coated in a desiccator for one hour using a vapor deposition protocol. This protocol was identical to the one employed to create the fluorocarbon-coated glass slides.

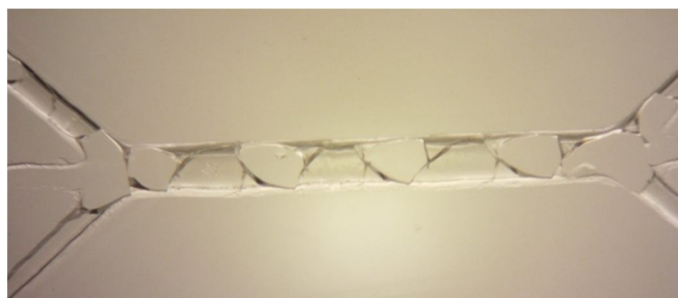


Figure 7. Cracked master structure.

2.A.3. Replica Molding

Conventional soft lithography techniques were used to create the polydimethylsiloxane (PDMS) microfluidic systems.³⁶ An 11:1 ratio of the base to curing agent from the PDMS elastomer kit (SkylardTM 184, Dow Corning) was used. The elastomer was thoroughly stirred or mixed, and then de-gassed using a vacuum pump and desiccator. If the mixture was not thoroughly mixed to establish homogeneity, the PDMS would not cure uniformly. However, this mixing process produces air bubbles, which if not removed can persist in the cross-linked structure; hence, the de-gassing step.

After being mixed and degassed PDMS was poured over a master structure for an approximate device thickness of ~1 cm and heated (~60°C, ~1 hour). The viscous liquid PDMS becomes a solid cross-linked polymer that can be easily peeled from the master structure. Master structures can be re-used multiple times with careful handling and cleaning. To re-use master structures any remaining PDMS was peeled off the master structure slide. Then this slide was washed in ethanol for 3 minutes followed by a distilled water rinse.

Access holes to channels were added using a 1.20 mm borer (Harris Uni-Core). To enclose the channels, the mold was placed onto a thin PDMS bottom. The PDMS channel portion and bottom portion were oxygen plasma cleaned, sealed together, and heated at $\sim 90^{\circ}\text{C}$ for roughly one hour to promote an irreversibly sealed device. Tubing was inserted into the channel access holes (Cole Parmer PTFE #24 Thin Wall Tubing Natural) (Figure 8). The insertion of tubing into these access holes often produced small cracks in the PDMS in the vicinity of these holes. These cracks enabled liquids being passed through the device to leak out of the device. To seal these leaks a small amount of uncured PDMS was first left at room temperature for ~ 4 hours. Then, small amounts of this PDMS was applied to each access hole of the device after which devices were placed in an oven (~ 30 minutes at 90°C) to promote PDMS curing. Allowing the PDMS to sit for several hours limits the viscosity of the PDMS and lowers the chance that the uncured PDMS will seep into the tubing, thereby clogging the tubing when it cures.

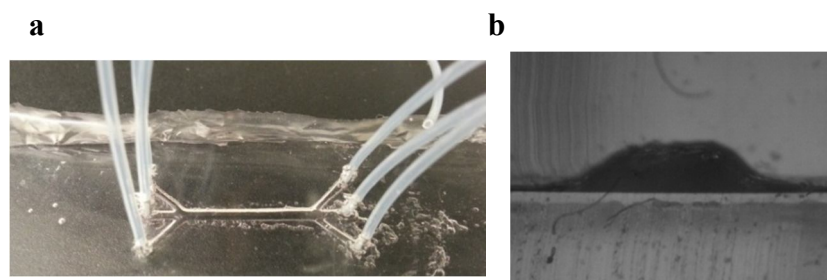


Figure 8. (a) PDMS mold with inserted channel tubing. (b) Optical image of cross-section of microchannel ($\sim 300\ \mu\text{m}$ high \times $15000\ \mu\text{m}$ long \times $800\ \mu\text{m}$ wide).

2.B. Device Operation

The goal was to operate the device in a regime where relatively little mixing between the input three streams occurred in the main channel. In this regime, a qualitative

agreement between the simulations* for this system and its actual operation was expected. To visually observe what flow rates, lead to this type of device operation, dye solutions were introduced into the system via the side streams prior to the entry of the crystal reagent solutions. Additionally, in order to be able to operate these prototypical PDMS devices for extended periods of time, bubble formation inside these devices (or their associated tubing) had to be eliminated. The occurrence of bubbles often alters the flow characteristic inside a device (Figure 9a). When the flow profile is changed undesirably, issues with experiment repeatability arise. Moreover, bubble formation can also cause the three streams to mix inside of the device causing rapid crystal formation during crystallization studies and, thereby, clogging the device. Thus, the protocol for operating these devices consisted of (1) procedures to minimize bubble occurrence, (2) a process to check flow characteristics, and (3) a method for forming and collecting crystals. Each of these protocols are detailed below.

2.C. Establishing Crystallization Protocol

2.C.1. Bubble Reduction

In order to minimize bubble occurrence, the source of the bubble interference had to be identified. It was determined that bubbles could enter the system via any open exposure to air. In particular, through the opening at the ends of channel tubing. In order to eliminate this exposure, syringe switching was done using a submerge technique. It was also determined that bubbles nucleated from inside the PDMS device at random times and locations. To eliminate this phenomenon, the entire device was first filled with

* Done by Dr. Kumi prior to the start of this study

ethanol using a syringe and then submerged in an ethanol bath. The submerged device was placed into a desiccator which was then evacuated (~20 minutes). This process removes air from the PDMS pores and infuses the PDMS with ethanol.³⁷ The device inlet tubes were connected to syringes (National Scientific Luer Lock Plastic-10 mL for outer tubes, 20 mL for center tube), and connected syringes were attached to pumps (New Era Pump Systems Model NE-1000). Ethanol was pumped through the outer channels at a flow rate of 120 $\mu\text{L}/\text{min}$. The flow rate for the center channel was 150 $\mu\text{L}/\text{min}$. During this ethanol flush (which was for ~5 minutes) the exit tubing was manipulated to ensure that ethanol was flowing out of all exit tubing and there were no air bubbles in the tubing or device (Figure 9b and c).

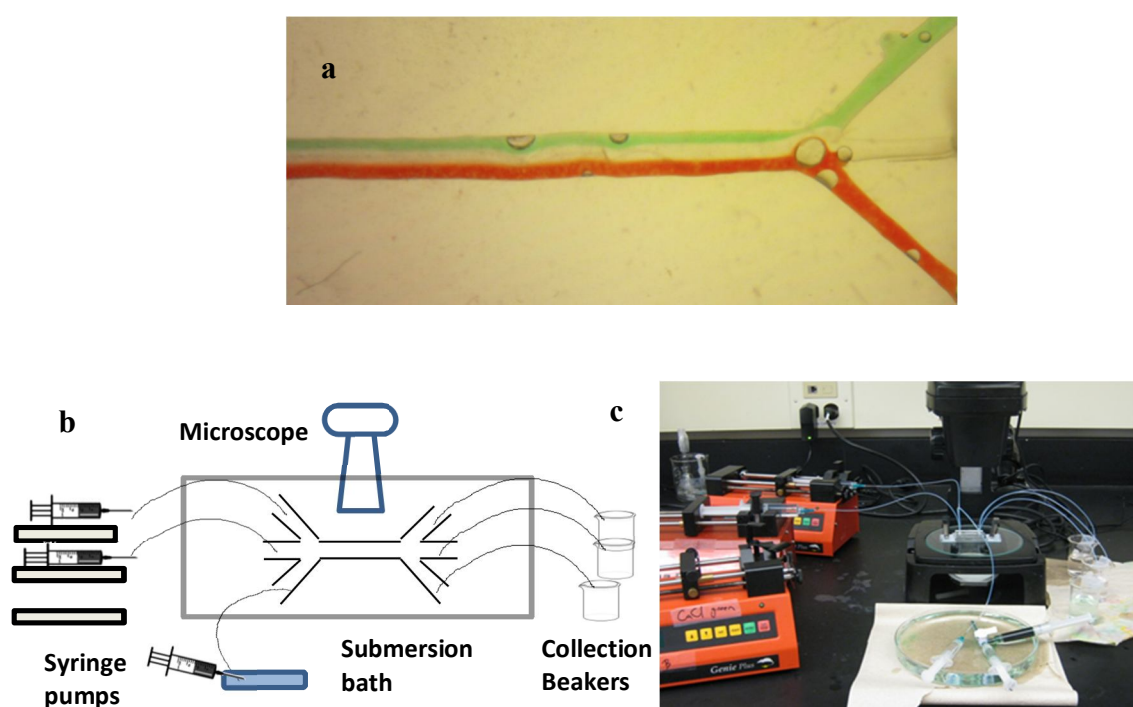


Figure 9. (a) Bubbles in the device that have altered fluid flow profile. (b) Schematic of experimental set up and (c) actual experimental set up.

2.C.2. Device Flow Characterization

After a device underwent bubble reduction procedures, the next step was to characterize the flow profile for the device. This characterization process consisted of a series of steps to ensure that a laminar flow profile could be established and maintained through a sequence of syringe switches. An image was recorded of the device prior to any dye fluid flow (Figure 10). The device was already connected to the syringe pumps for an ethanol flush as mentioned in the earlier section. The pumps were stopped to switch syringes containing ethanol to syringes containing the colored dye solutions. The method of syringe switching was to submerge the initial syringe and tubing into a large petri dish filled with distilled water. The tubing was removed from the initial syringe and carefully placed onto the next syringe to be used in the profile characterization while both syringes were underwater. The three ethanol syringes were replaced with one syringe containing a green dye solution, one containing a red solution and one containing distilled water. The dye solutions were used to visualize the flow of the side streams (i.e. stream widths). Distilled water remained the center fluid stream for the experiment. Syringes were returned to the pumps and flow was restarted at the rates of 120 $\mu\text{L}/\text{min}$ for the green and red colored solutions and 150 $\mu\text{L}/\text{min}$ for the water syringe. When the laminar flow profile was established, the rates were reduced to 20 $\mu\text{L}/\text{min}$ for the colored solutions and 50 $\mu\text{L}/\text{min}$ for the water.

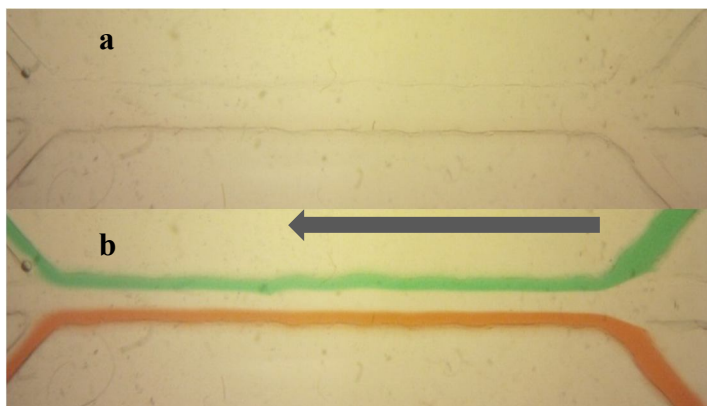


Figure 10. (a) Image of device prior to any dye fluid flow and (b) laminar flow profile of dye solution. Flow rates of the red and green are 20 $\mu\text{L}/\text{min}$ and center 50 $\mu\text{L}/\text{min}$. Arrow indicates direction of fluid flow.

To flush out the dye solution, pumps were stopped and syringes were switched to all water syringes. The same underwater protocol was conducted for all syringe switches. The flow rates remained the same (20 $\mu\text{L}/\text{min}$ outside channels; 50 $\mu\text{L}/\text{min}$ center channel) and at this point the experiment was referred to as “blind”. It could only be assumed that once the laminar profile had been established it would remain constant as the water cleared the dye solutions out of the device. When there was no evidence of colored solution, the syringes were switched once again to color to check that the profile was maintained. During these characterization trials each device was run for ~ 1 hour to ensure that there were no leaks or bubble occurrence then the device could be used for crystallization experiments.

2.C.3. CaOx crystallization

After a device was characterized for a reproducible flow profile, it was flushed with distilled water and set aside to be used in a CaOx crystallization experiment. To

begin a CaOx crystallization experiment a device underwent the bubble reduction protocol previously described. Then, a laminar flow profile was established and a switch to a blind experiment was made. At this point, an additional syringe switch was added to the protocol. Following the underwater switch protocol, the water syringes were switched to a CaCl_2 solution (previously green dye solution) and a $\text{K}_2\text{C}_2\text{O}_4$ solution (previously red dye solution). The salt solution concentrations used were always equal for this study. The salt concentrations investigated were: 20 mM, 40 mM and 60 mM. After the salt solution flow started, the device was monitored closely for any evidence of CaOx crystal formation. The strongest evidence of crystal formation in these experiments was the formation of a “salt line” (CaOx crystal line) in the center channel of the device (Figure 11). Microscopic images of the salt line formation were captured at various time intervals during the progression of the experiment.

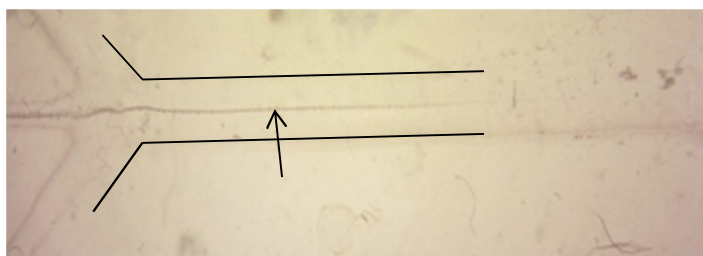


Figure 11. Image of “salt line” (CaOx crystal line) forming in the center channel of device. Arrow points to salt line forming in center channel.

2.C.4. Crystal Collection and Analysis

CaOx crystals formed in the device were collected into a saturated CaOx solution. The center collection beaker was switched to the saturated solution just before both colored solutions became completely clear (i.e., just before all the dye solution was

flushed out with water). The switch was made at this time so that the color profile could still be seen and adjusted if necessary. The best method for collection of crystals was to put a glass slide into the collection beaker. The glass slides were removed from the collection beaker at various time intervals to investigate any change in crystal shape or size over time. The glass slides were viewed under an optical microscope for evidence of crystal formation and collection. Optical images were taken of collected CaOx crystals to be characterized. Further characterization was done by SEM.

2.C.5. Establishing re-usability of device

After a crystallization experiment in a device was completed the device was flushed with water. Because of the low solubility of CaOx in water, water was unable to dissolve the CaOx crystals that had remained in the device within a suitable time frame, for example, 1 hour. Instead, a 2 M solution of HCl was used to clean the device of any remaining crystals. In order to confirm that the HCl flush was a successful method of cleaning out the devices, subsequent crystallization experiments were conducted in devices after the HCl flush. All previously discussed protocol was followed and the results of the experiments were compared to initial experiments for proof of reproducibility.

2.C.6. Additives (addition of NaPA)

Once the protocol and reproducibility of CaOx crystallization in a three-input, three-output continuous flow system had been established, the effect of polyacrylic ions on CaOx formation was investigated. Previous crystallization protocols were followed. The device was flushed with HCl, then it underwent the protocol for bubble reduction

and a laminar flow profile was established. During the syringe switches to water (“blind flow”) the center syringe was changed to a solution of sodium polyacrylate (NaPA). The effects of 1 mM, 5 mM and 10 mM concentrations of NaPA on CaOx crystallization in the microfluidic device were compared to previous experiments not containing any additive. Microscopic images of salt line formation and crystal collection were compared.

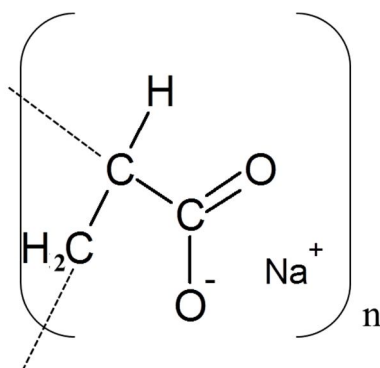


Figure 12. Structure of NaPA polymer.

Chapter 3: Results and Discussion

3.A. CaOx crystallization and analysis

Most CaOx crystallization experiments resulted in the formation of a dark line in the channel. To characterize this line, the two PDMS pieces of some devices (see Section 2.A.3) were separated after these devices were used for crystallization experiments. This separation provided better access to the aforementioned dark line and facilitated confirmation that this line was indeed a line of crystals, specifically CaOx crystals. Thus, the formation of a dark line of crystals was viewed as evidence that crystals were in fact forming via diffusion within the microchannel.

In order to determine the reusability of the devices used in this study, the goal was to conduct multiple experiments with the same device. However, initial replicate experiments lead to non-reproducible results. These non-reproducible results included, differences in the time of appearance of CaOx crystal line and a significant variation in the amount and type of crystals collected. Because devices were being re-used, there was a possibility that crystals remained in the channel even after the water flush at the end of the experiment. These remaining crystals could potentially affect any subsequent device usage by promoting aggregation. To eliminate this variability, a set of experiments were undertaken in which devices were used only once.

So as to ensure that the devices used in the aforementioned set of experiments had the same channel dimensions, these devices were made from the same master structure. The plan was to fabricate nine devices from each master structure so that triplicates of each input salt concentration (20, 40, and 60 mM) could be performed. Unfortunately, this strategy was difficult to implement because the production of each device appeared

to weaken the adhesion of the master structure to the substrate, and as a result master structures usually detached from the substrate before nine molds could be made (Figure 13). Thus, a different approach was adopted; the maximum number of molds (per master structure) were made and devices were completed following all previously discussed protocol (2.A.3). After devices were tested for leaks and laminar flow profile (see Device Operation 2.C.1-2) there were at least four usable devices per master structure. Therefore, quadruplicate experiments of each concentration input (20, 40, 60 mM) were conducted. Devices were labeled with a number, to represent master structure used, and a letter, specifying input concentration used (Table 3).

Master Structure	Concentration (40 mM)		
1	1A	1B	1C

	Concentration (mM)		
Master Structure #	60	40	20
2	2A	2B	2C
3	3A	3B	3C
4	4A	4A	4C
5	5A	5B	5C

Table 3. Labels used for devices discussed in this study specifying the master structure and concentration input used.



Figure 13. Damaged master structure after successive molds.

3.A.1. Establishing reproducibility using the same master structure

The first set of crystallization experiments (using devices molded from the same master structure) were conducted using equivalent (40 mM CaCl_2 and 40 mM $\text{K}_2\text{C}_2\text{O}_4$) salt concentrations. The initial profiles for all three devices (labeled as devices 1A, 1B, 1C) were relatively similar (Figure 14 (I)). The first sign of “salt line” formation occurred at similar times for each device in these 40 mM experiments (Figure 14 (II)). The line continued to grow and darken over time. At ~12 minutes the length of the salt line was similar for all three devices (Figure 15 (I)). The final profile check for all three devices suggested that laminar flow continued throughout the experiment (Figure 15 (II)). The outcome of the trials indicates that the results (appearance and growth of salt line) are reproducible when using devices made from the same master structure. Microscope optical images were taken frequently during the crystallization process. The images chosen for comparison purposes show similar salt line characteristics (length and darkness) at relatively close times; all times are relative to when the salt solutions are introduced into the device.

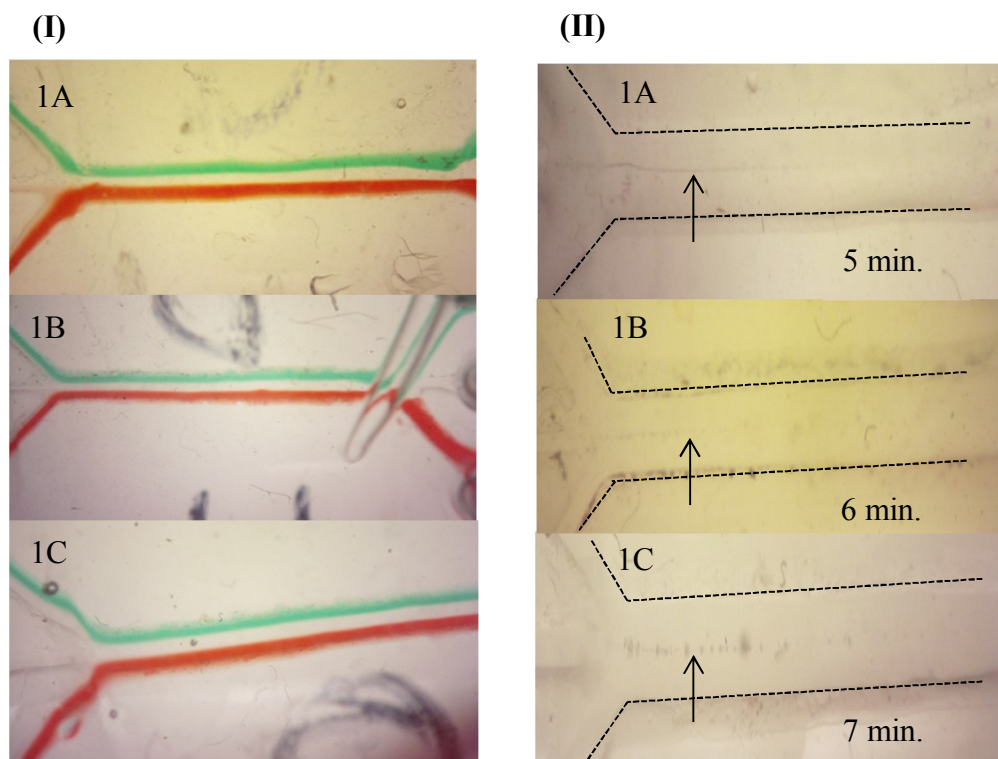


Figure 14. (I) The initial flow profiles of devices 1A, 1B and 1C are relatively similar. (II) After introducing the salts into the device, the first sign of CaOx formation in the device was 5 min. for device 1A, 6 min. for device 1B, and 7 min. for device 1C. Arrows point to where salt line is in the channel. The dashed lines depict the channel walls.

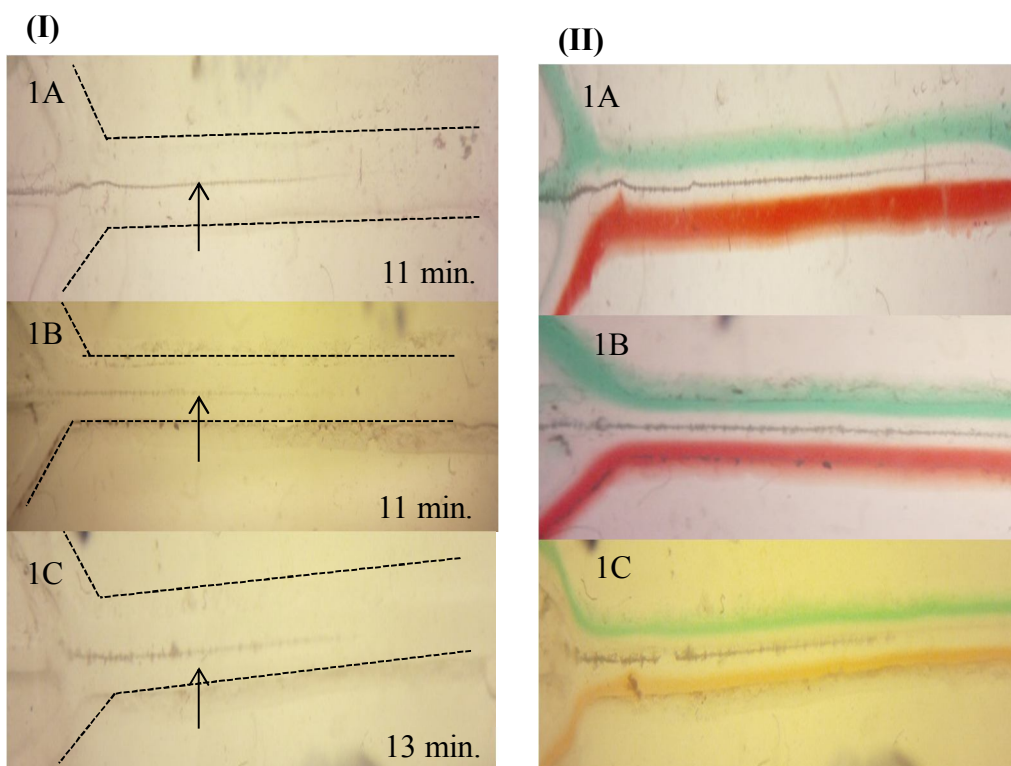


Figure 15. (I) The line continued to grow and darken over time. At ~12 min., the line was similar in length and darkness for all three devices. (II) The final profile check for all three devices suggests laminar flow remained throughout crystallization in the device. Arrows indicate where crystallization is evident in the channel. The dashed lines depict the channel walls.

Crystals collected from the experiments shown in Figures 15 and 16 had various shapes and sizes. Although, the X-shaped and prismatic COM crystals seemed dominant (Figure 16). Crystal collection was accomplished by placing a glass slide into the collection beaker, which contained a saturated solution of CaOx (see section 2.C.4). To determine if there was any change in size or shape of crystals collected over time, the glass slide present at the beginning of the experiment was removed from the saturated solution and replaced with a clean slide at 30 minutes. This replacement slide

was itself replaced after 15 minutes in solution (that is, 45 minutes total experiment time). Finally, a third slide replaced the second slide and was removed 15 minutes later (that is 60 minutes total experiment time). Slides were air dried and observed via an optical microscope. There did not seem to be any clear change in the size or shape of the crystals over time. Based on the habit of the crystals collected, crystallization produced COM and COD forms.

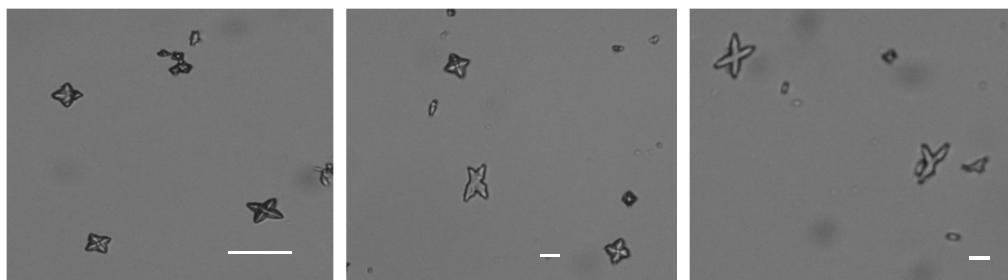


Figure 16. Microscopic images of crystal collection results. Representative images were chosen from device 1A, 1B, and 1C collections. Scale bars of optical images are 35 μm .

3.A.2. Establishing reproducibility using different master structures

After it was evident that experiments could be reproduced in different devices fabricated from the same master structure, the next goal was to examine the results of using devices molded from different master structures made from the same optical mask and using the same UV exposure conditions. While the overall dimensions of the microchannels in the molds were expected to be similar, it was unclear if different master structures from the same mask would have any microscopic variations (that would be imparted to the molds made from these masters) significant enough to influence reproducibility.

3.A.2.a. 60 mM concentration inputs

First, a set of 60 mM input salt concentration experiments were tested in devices fabricated from different master structures; these devices are hereafter referred to as Devices 2A, 3A, 4A, and 5A. The salt line appeared at 4 minutes (2A), 5 minutes (3A), 5 minutes (4A) and 7 minutes (5A) after introducing salts into these devices (Figure 17 a (I)). At about 9 minutes after salt introduction the line had lengthened and darkened (Figure 17 a (II)). The line continued to grow and darken until about 14 minutes (Figure 17 a (III)). The line did not seem to change much past that time frame. The crystal collection protocol was followed by placing a glass slide in the collection beaker at the beginning of the experiment. The collection glass slide was removed and/or replaced at 30 minutes, 45 minutes and 60 minutes after salt solution pumps were started. Thus, the first slide collected crystals that formed within the first 30 minutes, while the slide that replaced it (i.e. the one removed 45 minutes after the salts were introduced) collected crystals that formed in the subsequent 15 minutes. There was no discernable difference in size, shape, or quantity of crystals collected as time passed. Each slide had a mixture of COM and COD shapes, although there were very few COD crystals (Figure 17 b). The quantity of crystals collected on each slide was inconsistent. However, based on the salt line characteristics at different times (length, darkness), the results of this set of experiments suggested that using master structures from the same optical mask to fabricate a device leads to results that are relatively the same.

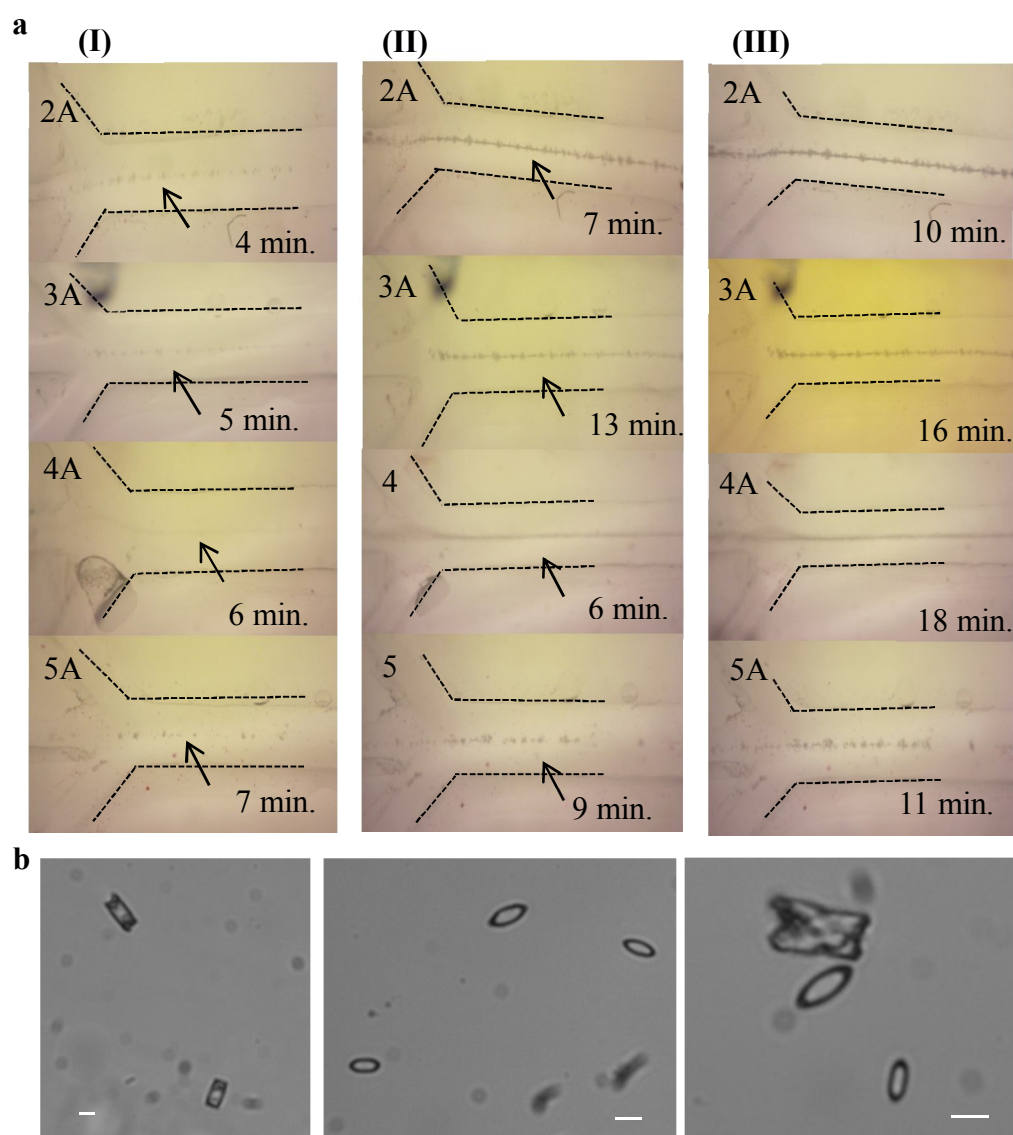


Figure 17. (a) 60 mM input concentration comparisons. (I) Salt line appearance: 4 min.(2A), 5 min.(3A), 5 min.(4A), and 7 min.(5A). (II) Salt line growth: 7 min.(2A), 13 min.(3A), 6 min.(4A), and 9 min.(5A). (III) Salt line growth: 10min.(2A), 16 min.(3A), 18 min.(4A), and 11 min.(5A). Arrows indicate where crystallization is evident in the channel. (b) Representative collection of 60 mM input concentration CaOx crystals. Scale bars of optical images are 35 μ m.

3.A.2.b. 40 mM concentration inputs

For experiments using 40 mM salt concentrations in devices fabricated from different master structures (hereafter referred to as Devices 2B, 3B, 4B and 5B), the salt line appeared ~7 minutes after the salt syringe switch in three out of the four devices. In one device (Device 4B) the line was not evident until ~16 minutes (Figure 18 a (I)). As mentioned previously there is some variability when it comes to the devices and master structures, so this may have contributed to the difference in the time it took for the line to emerge. It is also possible that the line appeared at a sooner time but could not be seen at ~7 minutes. Device thickness, illumination parameters[†], or pump start-up traits (see Appendix) are variables that could lead to deviation in the time that a salt line appeared; that is, could be visibly seen on the microscope image.

As with the 60 mM concentration experiments, the line continued to grow and darken over time (Figure 18 a (II and III)). The line did not change much after about 40 minutes. The collection slides were removed at 30, 45, and 60 minutes. Surprisingly, the number of crystals collected from these experiments was small relative to the 60 mM experiments (Figure 18 b). There were no crystals recovered from one particular device (Device 2B). The identifiable shapes collected were a mixture of COM and COD, but minimal COD were identified. There did not appear to be a change in shape or size over time. Like the 60 mM experiments, the results of the 40 mM concentration trials also suggest that using devices made from the same master structure will produce reproducible results of salt line appearance time and increase in length of the line over time.

[†] Room lighting, or microscope lighting

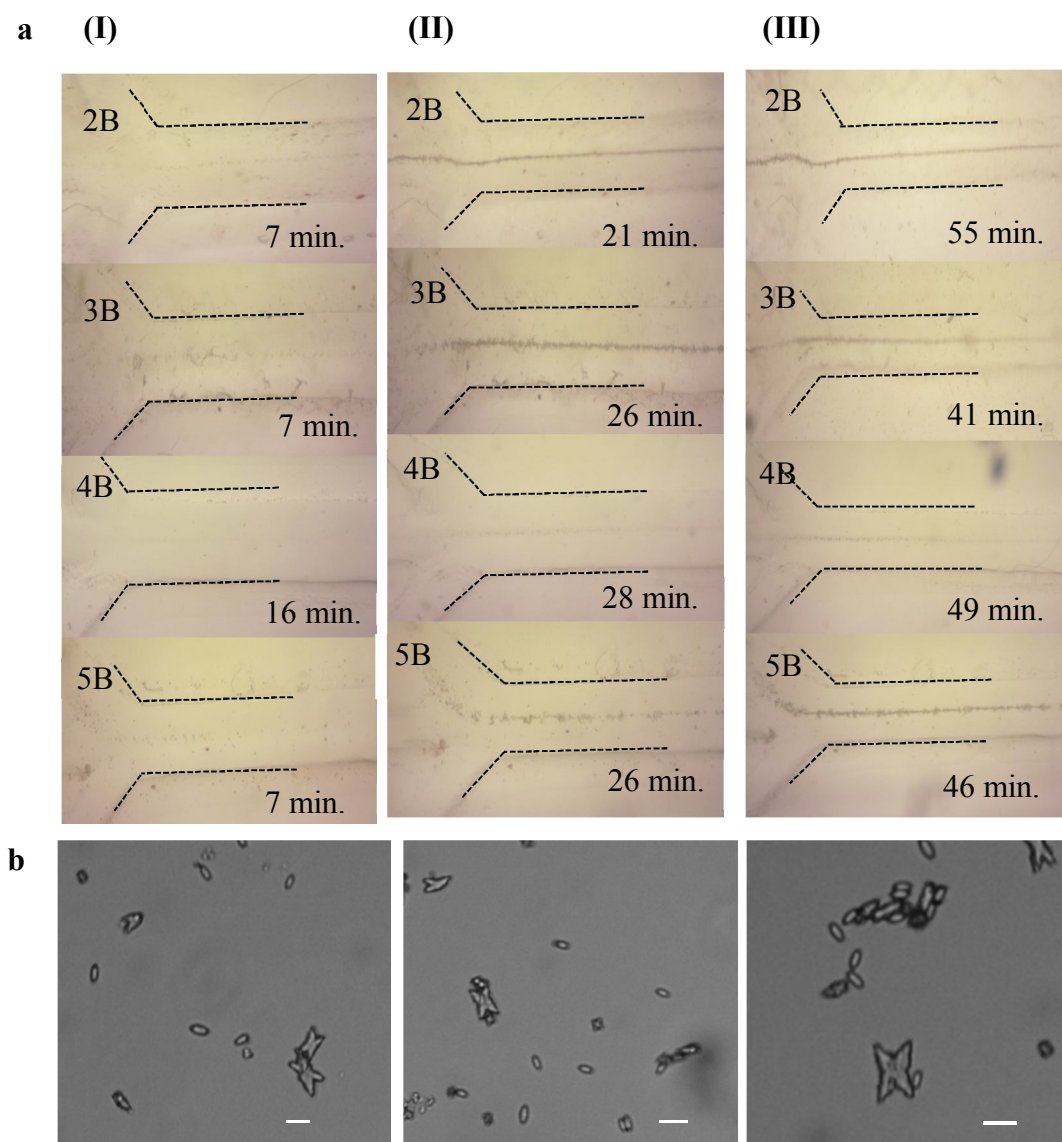


Figure 18 (a) 40 mM input concentration comparisons. (I) Salt line appearance: 7 min.(2B), 7 min.(3B), 16 min.(4B), and 7 min.(5B). (II) Salt line growth: 21 min.(2B), 26 min.(3B), 28 min.(4B), and 26 min.(5B). (III) Salt line growth: 55 min.(2B), 41 min.(3B), 49 min.(4B), and 46min.(5B). (b) Representative collection of 40 mM input concentration CaOx crystals. Scale bars of optical images are 35 μm .

3.A.2.c. 20 mM concentration inputs

Experiments were also conducted using 20 mM input concentration of salts in devices made from different master structures; hereafter referred to as Devices 2C, 3C, 4C and 5C. The salt line in Device 2C was very faint and not evident until 30 minutes after salt solution introduction. In Device 3C the line was also faint and could be detected at 20 minutes after salt solution introduction (Figure 19 a (I)). In the other two devices (4C and 5C) a faint line was not visible until 40 and 50 minutes after salt introduction. The line in Devices 2C and 3C darkened and lengthened over time, with no discernable change seen after 50 minutes (Figure 19 a (II)). As with previous experiments, collection slides were removed from the collection beaker at 30 and 45 minutes after salt solution start and replaced with clean slides. The final slide was removed 60 minutes after the start of the salt solution pumps. There were no visible crystals collected from the experiment in Device 5C. A mixture of COM and COD crystals were detected on the slides from the other trials (Figure 19 b, c). There were no X-shaped COM crystals detected in any of the collections from this set of experiments. There did not appear to be any difference in the size or shape of the crystals, with time. The results of the 20 mM concentration trials also suggest that results using devices made from different master structures will be similar.

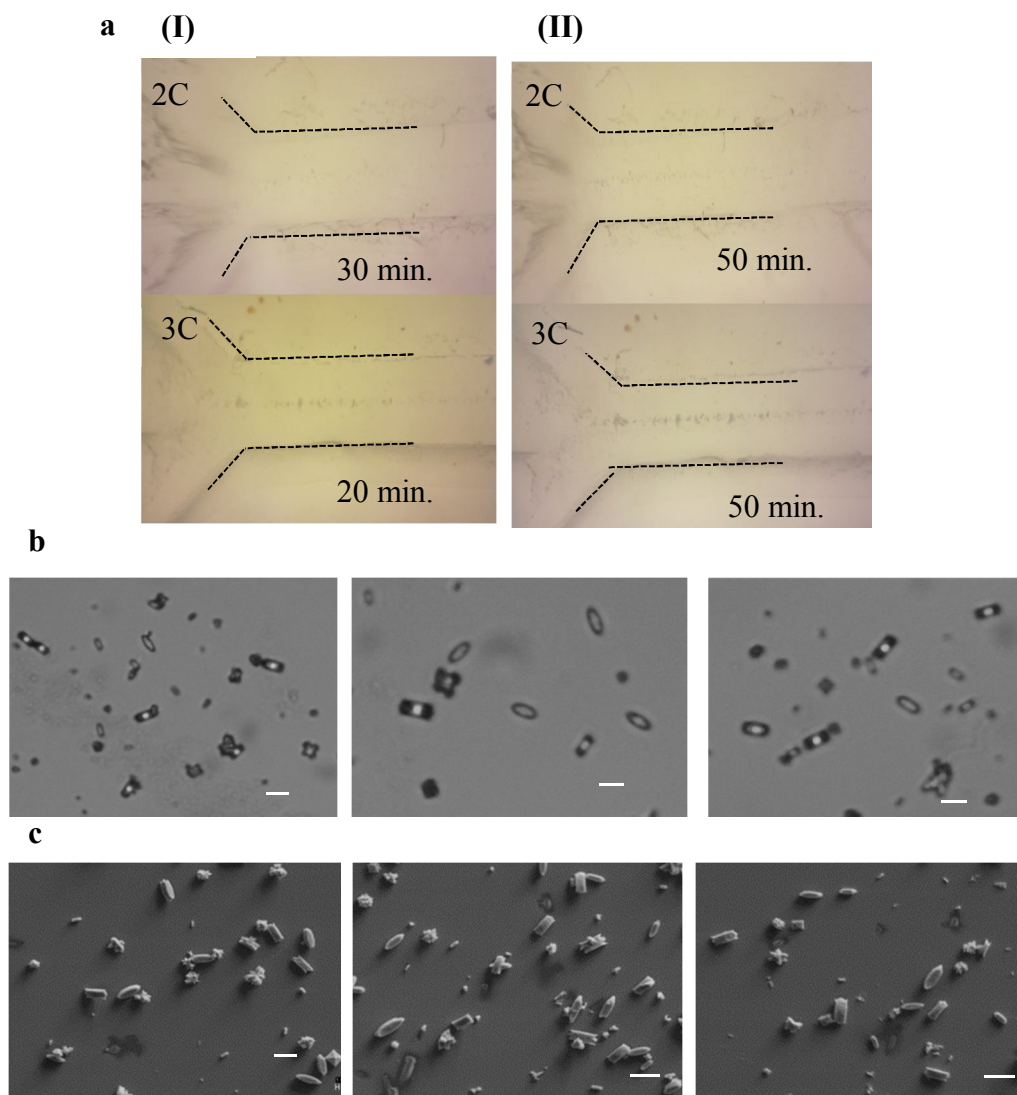


Figure 19. (a) 20 mM input concentration (I) Salt line appearance at 30 min. (2C) and 20 min. (3C). (II) Salt line at 50 min. (2C,3C). (b) Optical images of representative collection of 20 mM input concentration CaOx crystals. Scale bars of optical images are 35 μm . (c) SEM images of representative collection of 20 mM input concentration CaOx crystals. Scale bars of SEM images are 10 μm .

3.A.3. Summary of results

Due to the concern of the variability of the master structures made from the same optical mask, it was necessary to compare results of studies using devices fabricated with different master structures. The results of these experiments prove that reproducibility is possible in devices that have been fabricated from different master structures. Although the salt line may have looked different in some of the devices, the time of appearance, length of line, and crystal collection results were relatively the same for the same concentration. However, there was a clear difference in results between the different concentrations.

3.B. Concentration Comparisons

The average time of salt line appearance for 20 mM equivalent input concentrations of salts was 35 minutes, while the average time of salt line appearance for 40 mM equivalent input salt concentration experiment was 9.25 minutes. For the 60 mM equivalent input salt concentration, the average time of line appearance was 5.25 minutes. As the input concentration of salts was increased the time of line appearance decreased and the length of the line increased (Figures 20 and 21). The salt line was first evident toward the end of the channel and lengthened in the opposite direction of fluid flow.

3.B.1. Summary of results

The higher the ion concentration diffusing into the center stream, the less time it takes for saturation to occur in the center stream. This is why the salt line was seen sooner for the higher concentrations. However, the ion concentration needed for crystallization in the center stream was achieved toward the end of the channel. As fluid

flow continued, the ion concentration in the center stream increased causing nucleation and aggregation to occur. This is why the salt line lengthened and darkened opposite the direction of fluid flow. It is surprising the 20 mM input concentration led to such a larger difference in appearance time. It was suspected that the 20 mM input concentration would lead to a salt line appearance at ~13 minutes due to the difference in times of the 40 and 60 mM concentrations (~9 minutes and ~5 minutes). It is possible that the 20 mM input concentration salts were forming crystals sooner than the observed 35 minutes but were not big enough to be seen. It is also possible that there were not many crystals attached to the surface of the channel for the 20 mM concentrations.

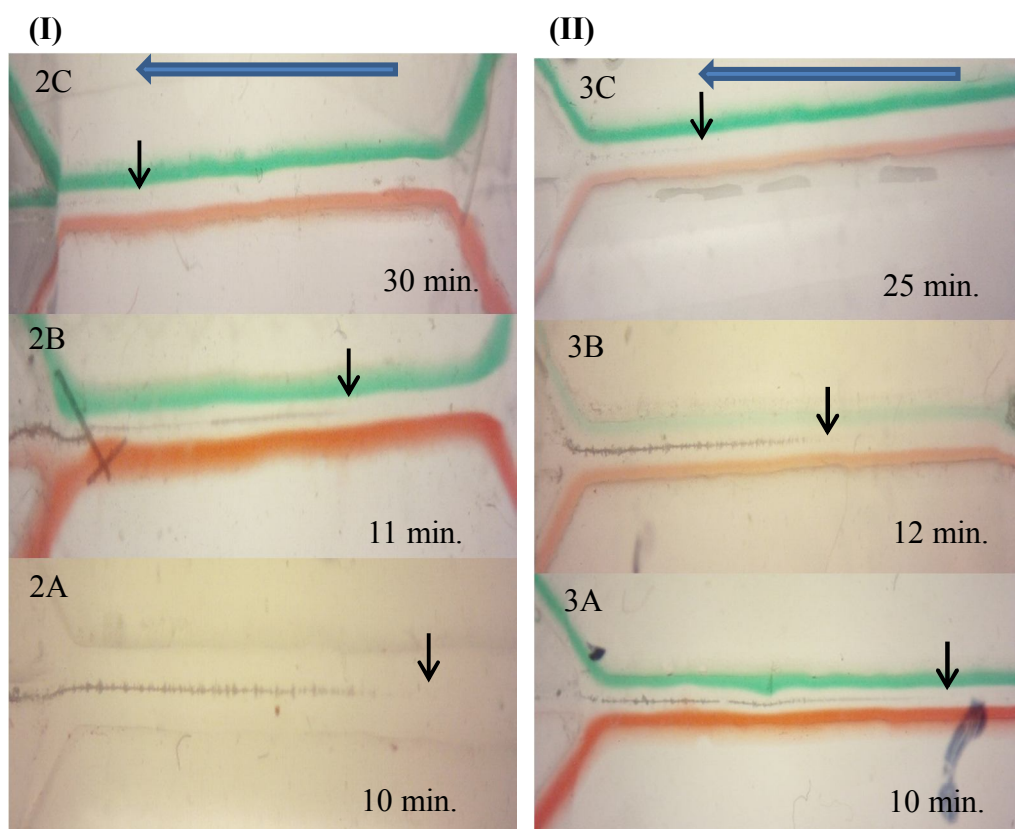


Figure 20. Comparison of salt line darkness and growth over time. (I) Device 2A (20 mM), 2B (40 mM), 2C (60mM). (II) Device 3A (20 mM), 3B (40 mM), 3C (60 mM). Vertical arrows indicate the end of salt line growth in center channel. Horizontal arrows indicate fluid flow direction.

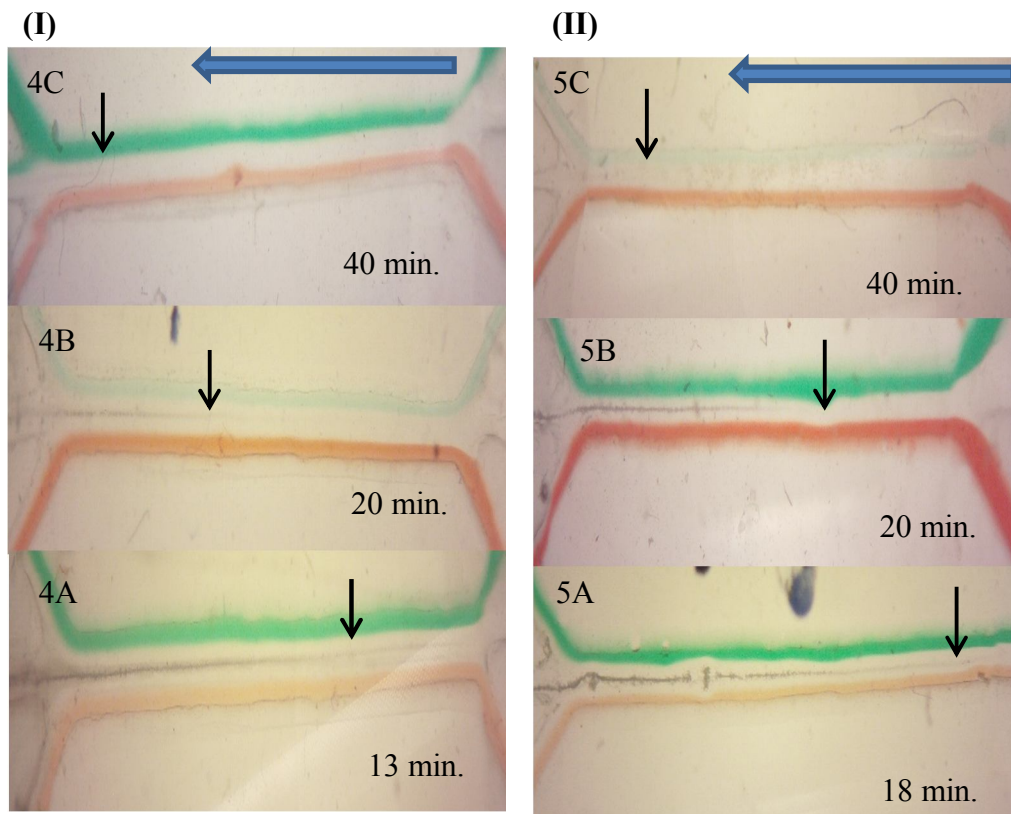


Figure 21. Comparison of salt line darkness and growth over time. (I) Device 4A (20 mM), 4B (40 mM), 4C (60 mM). (II) Device 5A (20 mM), 5B (40 mM), 5C (60 mM). Vertical arrows indicate the end of salt line growth in center channel. Horizontal arrows indicate fluid flow direction.

3.C. Use of HCl as a solvent

One of the benefits of using a microfluidic device is cost efficiency. The more times a device can be used the more cost effective this method becomes. After each previously discussed experiment, there were crystals still in the device, even after the water flush (see Section 2.C.5) (Figure 22 a). Using a solvent that will effectively clean out any leftover crystal residue will extend the use of each device. A 2 M solution of HCl

was used to flush all previously used devices in this study. After the HCl flush there did not appear to be any crystals left in the devices (Figure 22 b). To test the efficacy of HCl as a solvent all experiments were repeated so ensure that HCl did not alter the crystallization process.

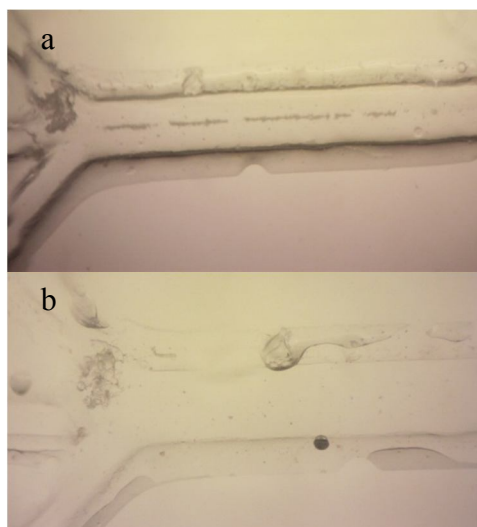


Figure 22. (a) Microscopic optical image of Device 3B before HCl flush. Device had crystals left in the channel after experiment and water flush. (b) Device 3B after HCl flush. Crystals appear to be removed completely. This image is representative of the same results for all other devices.

3.C.1.a. Device 2 comparisons before and after HCl

The results from all experiments before using HCl, to clean the device, will be referred to as “before HCl”. The results after using HCl, to clean the device, will be referred to as “after HCl” for comparison. The first evidence of salt formation in Device 2A (60 mM) for the “before HCl” trial was at 5 minutes compared to 6 minutes for “after HCl” trial. Similar to the “before HCl” trial the line continued to darken and grow over

time for the “after HCl” trial (Figure 23 a-d). The first evidence of crystal formation in Device 2B (40 mM) occurred at 7 minutes (“before HCl”) and 6 minutes (“after HCl”). The salt line continued to darken and lengthen over time for both sets of trials (Figure 24 (I) a-d). For Device 2C (20 mM), the “after HCl” device appeared to have little, if any, crystals in the device which were the same results as the “before HCl” trial after 60 minutes. (Figure 24 (II) a,b).

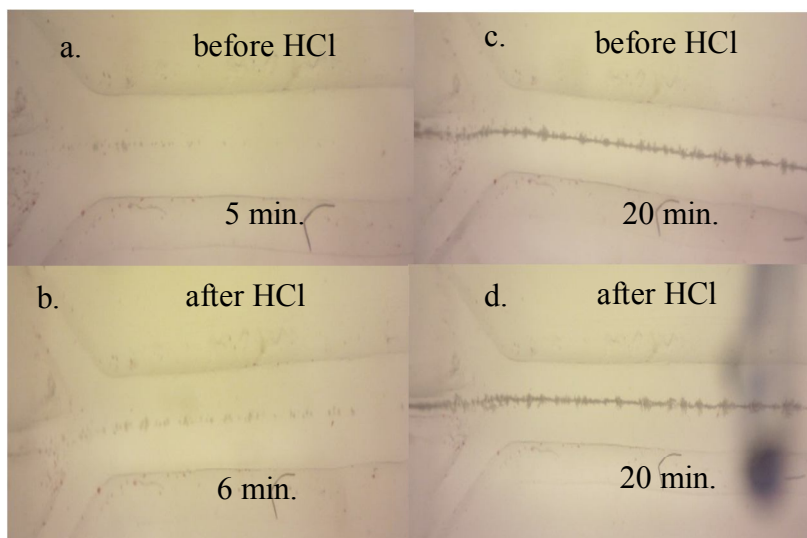


Figure 23. Initial (a, b) and final (c, d) appearance of salt line for the “before HCl” and “after HCl” experiments using Device 2A.

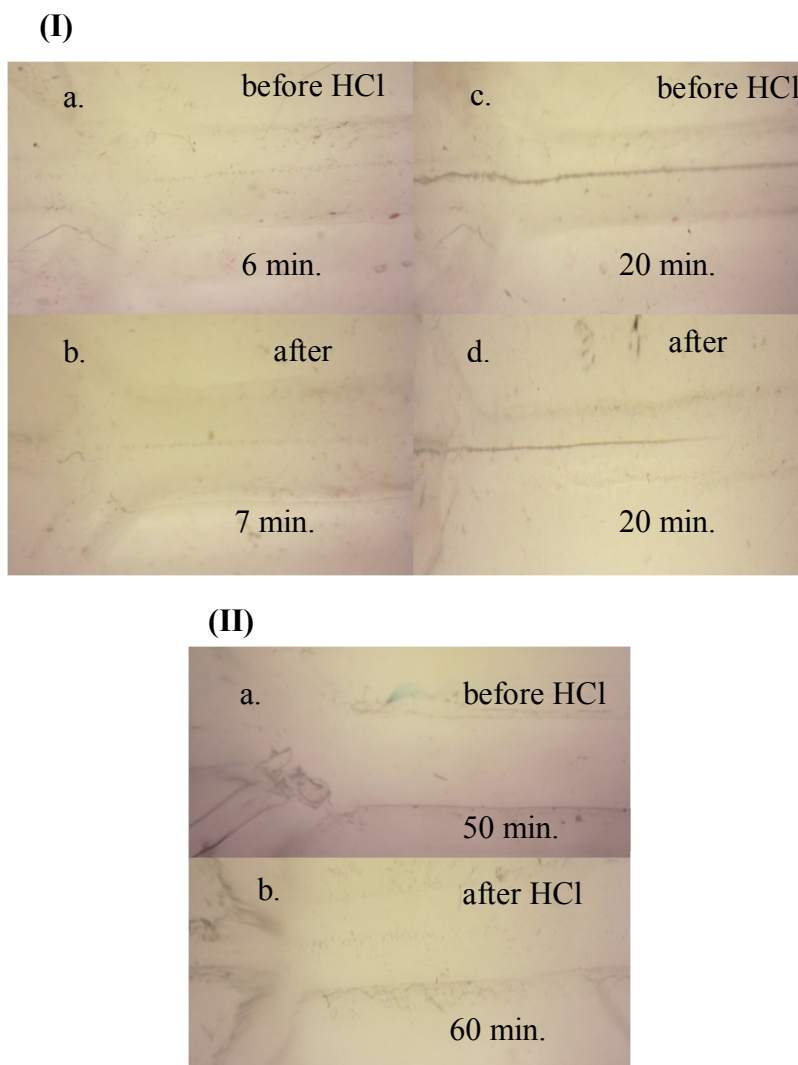


Figure 24. Initial (a, b) and final (c, d) appearance of salt line for the “before HCl” and “after HCl” experiments using devices made from master structure 2. Images for (I) Device 2B, (II) Device 2C.

3.C.1.b. Device 3 comparisons before and after HCl

For Device 3A (60 mM) the appearance of the salt line occurred at 4 minutes for the “before HCl” trial and 5 minutes for the “after HCl” trial. The salt line continued to darken and lengthen over time. After 20 and 30 minutes the salt line appeared the same

for both the “before HCl” trial and the “after HCl” trial respectively (Figure 25 a-d). In Device 3B (40 mM) the salt line appeared at 7 minutes for the “before HCl” trial and 8 minutes for the “after HCl” trial. The salt line continued to darken and lengthen over time similarly for both the “before HCl” and “after HCl” trial (Figure 26 a-d). Device 3C (20 mM) could not be tested using the HCl flush method. During the HCl flush the device started leaking. The top and bottom PDMS pieces of the device were no longer properly sealing the channels of the device. Attempts to re-seal these top and bottom components of this device were unsuccessful.

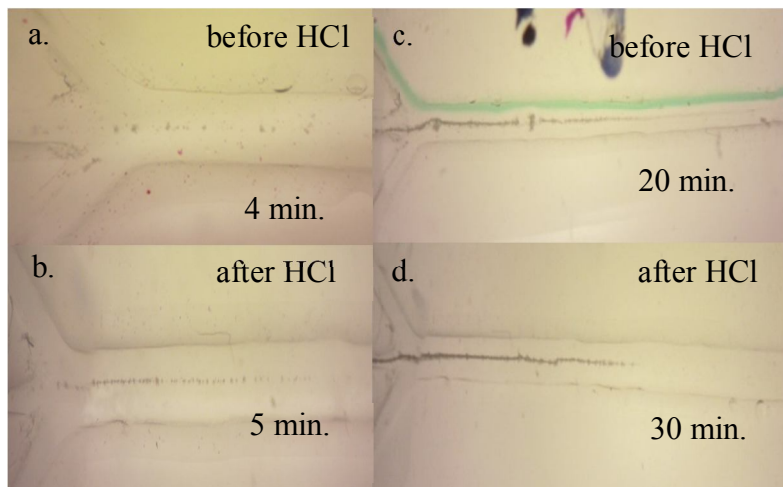


Figure 25. Initial (a,b) and final (c,d) appearance of salt line for the “before HCl” and “after HCl” experiments using Device 3A.

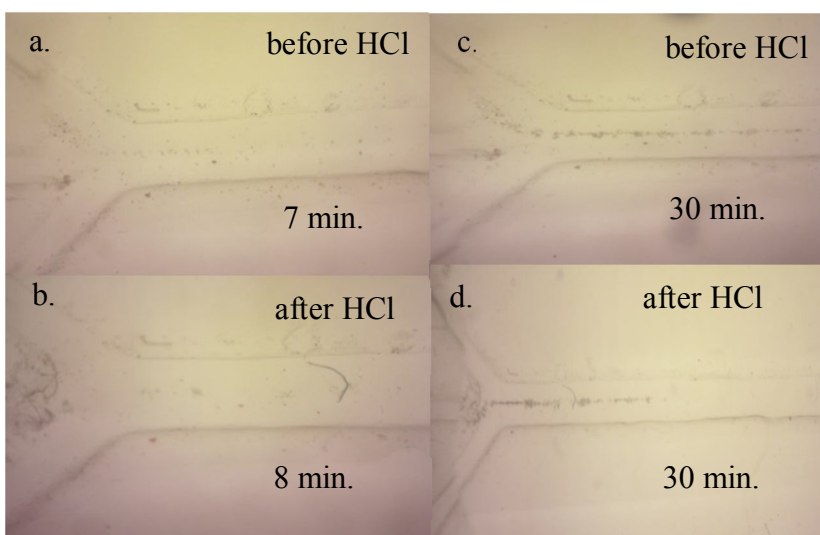


Figure 26. Initial (a,b) and final (c,d) appearance of salt line for the “before HCl” and “after HCl” experiments using Device 3B.

3.C.1.c. Device 4 comparisons before and after HCl

For both the “before HCl” and the “after HCl” trials the line was seen at 5 minutes for Device 4A (60 mM). The line appeared to darken and lengthen over time and was relatively the same at ~20 minutes after introduction of salts into the device (Figure 27 (I) a-d). In Device 4B, the salt line was evident at 16 minutes for the “before HCl” trial and 8 minutes for the “after HCl” trial. The salt line continued to darken and lengthen over time and looked relatively the same after 30 minutes (Figure 27 (II) a-d). For Device 4C (20 mM) the salt line was not evident until 60 minutes for the “before HCl” trial and after 60 minutes there was no clear line for the “after HCl” trial (Figure 27 (III)).

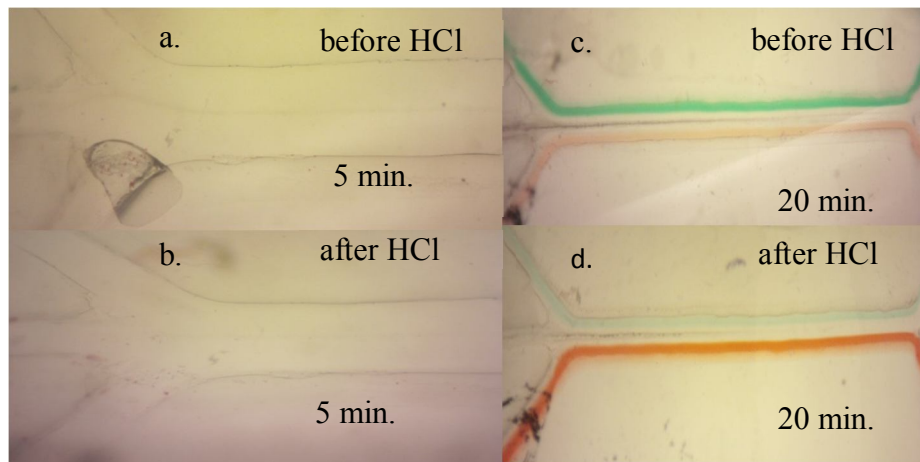
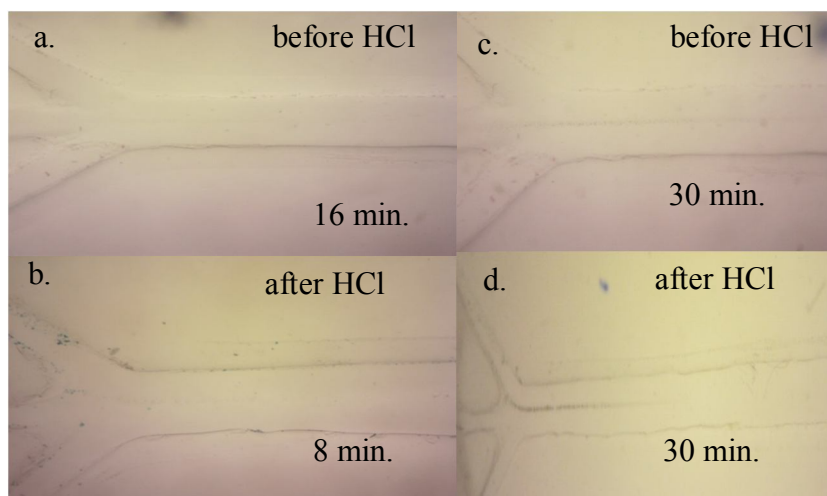
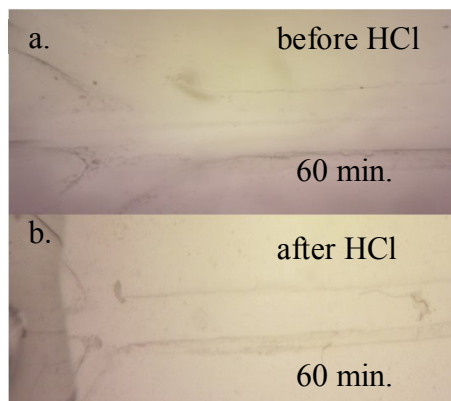
(I)**(II)****(III)**

Figure 27. Initial and final appearance of salt line for the “before HCl” and “after HCl” experiments using devices made from master structure 4. Images for (I) Device 4A, (II) Device 4B and (III) Device 4C.

3.C.1.d. Device 5 comparisons before and after HCl

For Device 5A (60 mM) the salt line first appeared at 7 minutes for the “before HCl” trial and 4 minutes for the “after HCl” trial. The salt line continued to darken and grow over time (Figure 28 a-d). The salt line appeared at 7 minutes for the “before HCl” trial and 8 minutes for the “after HCl” trial in Device 5B (40 mM). The salt line continued to darken and lengthen over time as with all the other 40 mM trials (Figure 29 (I) a-d). For Device 5C (20 mM) the salt line became evident after about 40 minutes for the “before HCl” trial, however a salt line was not seen after 60 minutes for the “after HCl” trial (Figure 29 (II) a,b).

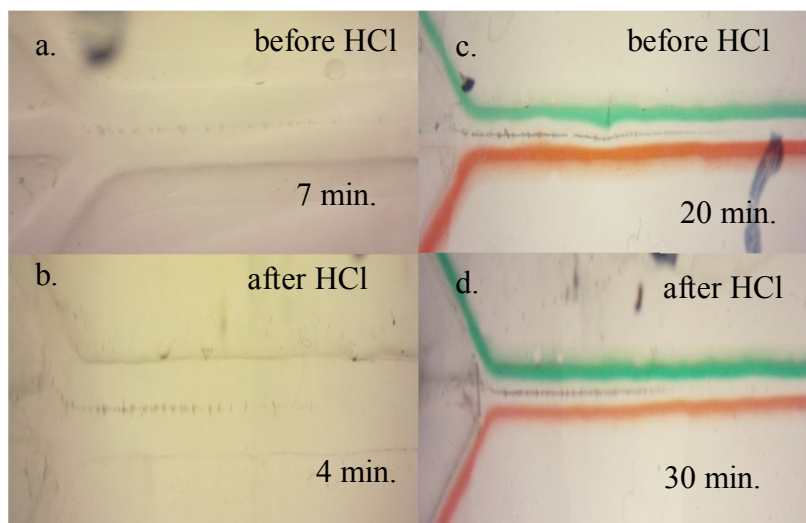


Figure 28. Initial (a,b) and final (c,d) appearance of salt line for the “before HCl” and “after HCl” experiments using Device 5A.

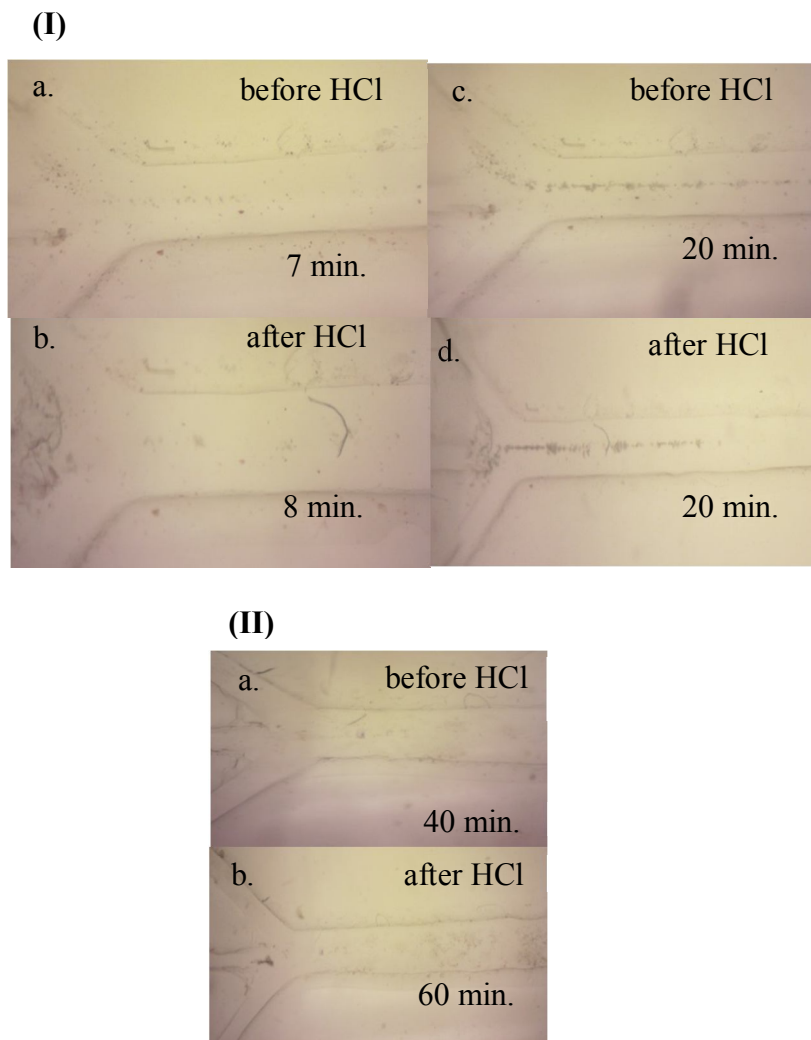


Figure 29. Initial (a,b) and final (c,d) appearance of salt line for the “before HCl” and “after HCl” experiments using devices made from master structure 5. Images for (I) Device 5B and (II) Device 5C.

3.C.2. Summary of results

Based upon the results of the trials using HCl as a solvent, it has been proven that HCl is a suitable solvent to clean out a device after running a crystallization experiment. After using HCl to flush a device the line appearance time per input salt concentration was relatively the same as initial experiments. The characteristics of salt line growth and

darkening were also repeatable. By using HCl as a solvent, results can be reproduced without having to use multiple different devices.

3.D. Effects of additive on CaOx crystallization

Previous studies have shown that specific polymeric additives inhibit CaOx growth.³⁸ The 60 mM input concentration trials always showed evidence of a salt line using water as the middle stream. This concentration also took the least amount of time to see results. This was seen as the most reliable concentration choice to use for additive tests. The set of devices used for the additive trials were fabricated from the same master structure (referred to as master 6). These devices had not been previously used in any other crystallization experiments. These devices will be referred to as “6” followed by “P” (polyacrylate) and the concentration of additive that was used.

3.D.1.a. 1 mM NaPA

The first concentration of sodium polyacrylate (NaPA) that was added to the center stream of the device was 1 mM. The salt line was first seen at 5 minutes after adding the 60 mM input salt concentrations. This is very comparable to the other 60 mM trials in which the first evidence of salt formation was on average 5 minutes (Figure 30 (I)). The salt line continued to darken and lengthen over time; however, the line did not get as dark or long as the trials without additive (Figure 30 (II)). Optical microscope images show that the CaOx formed with NaPA added are rounded and dumbbell-shaped. SEM images confirm dumbbell-shaped CaOx were formed (Figure 30 (III, IV)).

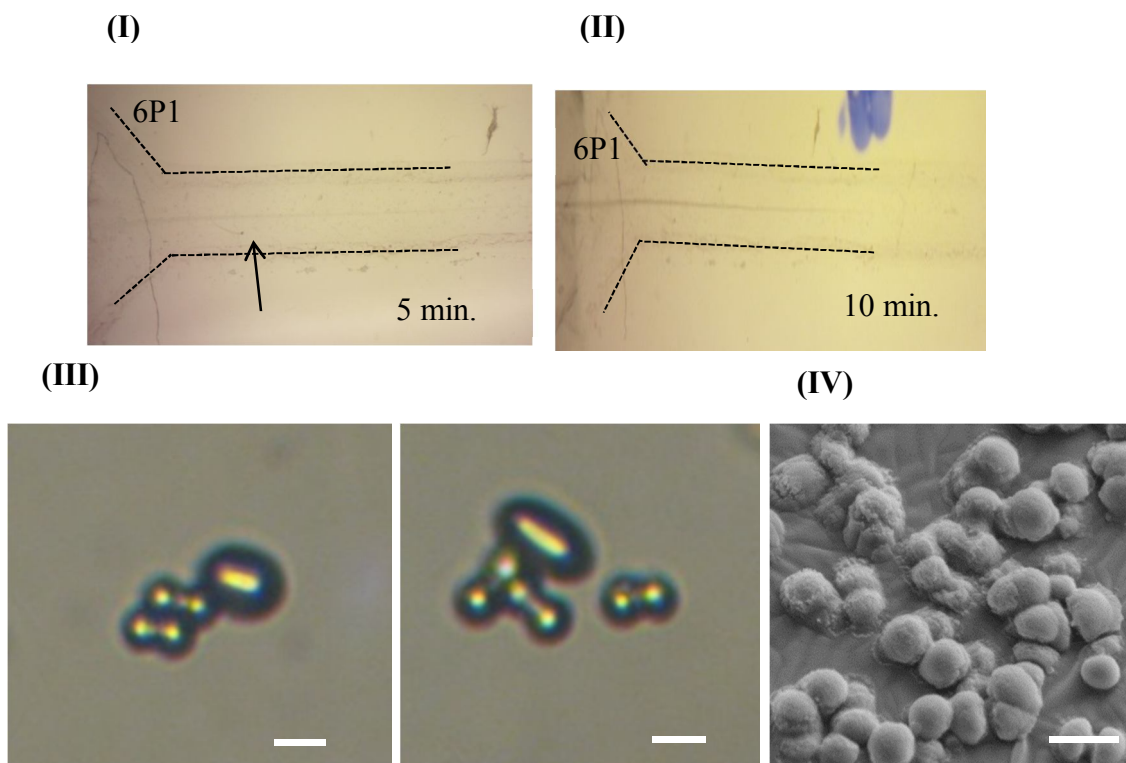


Figure 30. (I) Salt line appeared at 5 min. for 60 mM input concentration with 1 mM NaPA (6P1). (II) Line continued to grow over time but not as much as without additive. (III) optical and (IV) SEM images of CaOx formed with addition of 1 mM NaPA. Optical images scale bar is 10 μ m SEM scale bar is 5 μ m

3.D.1.b. 5 mM NaPA

The next concentration of NaPA screened was 5 mM. The first sign of salt line formation occurred at 8 minutes after addition of the 60 mM input salt concentrations. This is slightly higher than the average of 5 minutes for all other 60 mM trials conducted (Figure 31 (I)). The line continued to darken and lengthen over time. However, it did not get as long as the other 60 mM trials conducted (Figure 31 (II)). There were no crystals collected from this experiment.

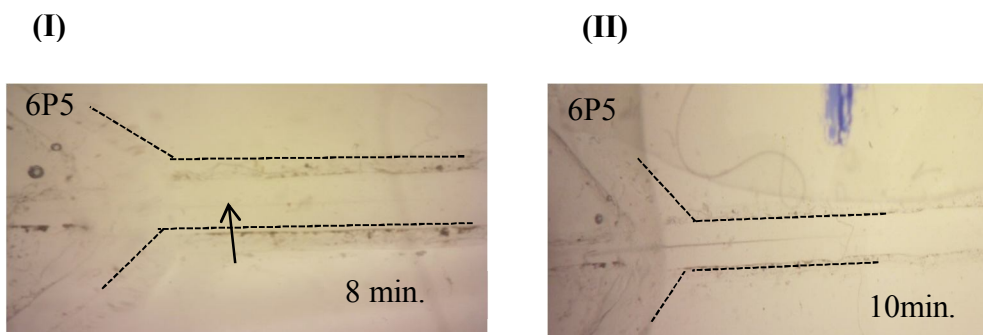


Figure 31. (I) Salt line appeared at 8 min. for 60 mM input concentration with 5 mM NaPA (6P5). (II) Salt line for 5 mM NaPA additive not as dark or long as the other trials.

3.D.1.c. 10 mM NaPA

The last concentration of NaPA tested was 10 mM. After 20 minutes there was no evidence that a salt line had formed in the channel. This is significantly different than the 60 mM trials without additive. Since there was no evidence of salt line formation there is not a comparison of lengthening or darkening of the line for 10 mM additive (Figure 32). There were no crystals collected from this experiment.

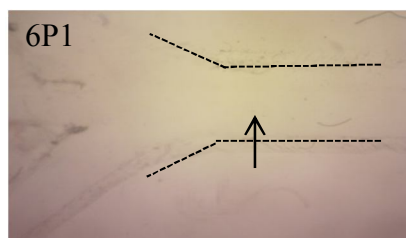


Figure 32. A salt line was not evident in the channel after 20 min. using the 10 mM NaPA additive (6P10).

3.D.2. Summary of results

The results of the additive trials indicate that NaPA does, in fact, impact the formation of CaOx in a microfluidic device. First, the 1 mM NaPA addition produced dumbbell shaped crystals as opposed to previously collected the X-shaped and prismatic shaped COM crystals without additive. These results support previous studies that show polyelectrolytes, such as polyacrylate ions, adhere to crystal faces and alter CaOx habit.³⁸ As the concentration of NaPA increased the time of salt line appearance also increased (Figure 33). The increased concentration of additive could be altering the concentration gradient of ions to the center stream thereby inhibiting formation of crystals in the center stream. It is also possible that the crystal habit is altered to an extent that aggregation is minimal, if existent.

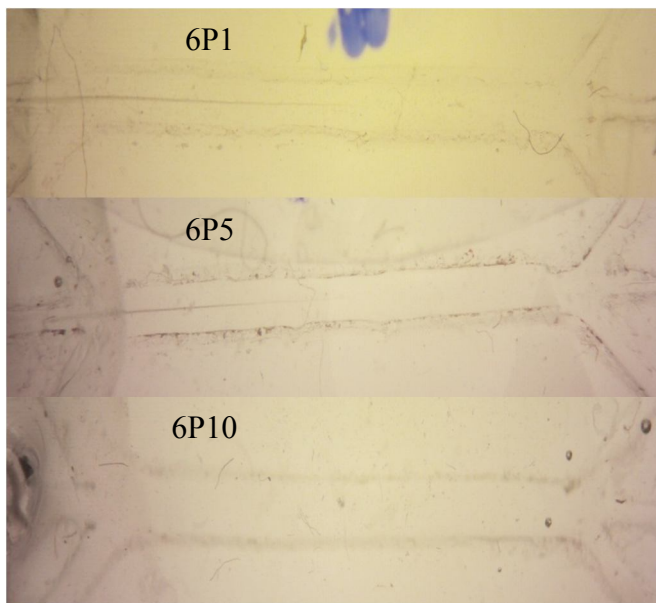


Figure 33. (a) 1 mM, (b) 5 mM, (c) and 10 mM NaPA concentration comparison after 20 min.

CHAPTER 4: Future Work

This study used a three-stream design in which Ca^{2+} and $\text{C}_2\text{O}_4^{2-}$ ions diffused into a center stream where crystallization occurred. Microfluidic devices were fabricated using soft lithography techniques. A reproducible protocol was established for making and operating the device as well as protocols for multiple use of devices. CaOx crystals formed in the center channel, and these crystals were collected and analyzed. Equivalent input concentrations of 20, 40 and 60 mM were studied. It was found that, as the input concentration of salt solutions increased the time for the line to appear in the channel decreased. It was also determined that the higher the concentration of input salt solutions the darker and longer the line became. CaOx crystals collected were a mixture of COM and COD.

Several studies have been done using additives that mimic urinary proteins that may inhibit crystal growth or adhesion to the renal tubules.^{9,14,15,17,18} NaPA was the additive used in this study. The concentrations of NaPA used in this study were 1, 5, 10 mM. As the concentration of NaPA increased the time it took for the line to appear increased and the length and darkness of the line decreased. NaPA has been reported to alter crystal shape from prismatic to dumbbell.³⁹ The crystals collected from the additive studies did, in fact, produce dumbbell or rounded shape crystals.

One of the problematic issues in this study was the variability in crystal collection. It was difficult to position the glass collection slide so that the crystals exiting the middle stream outlet tubing would fall onto the slide. In many of the experiments reported in this study, it was difficult to keep this middle stream outlet tubing at the

center of the collections slide during crystal formation. In fact, the exit of this tubing tended to reside near the edge of the crystal collection slide. The variability in crystal collection made it difficult to find crystals on the collection slide and make comparison between the properties (forms and habits) and amounts of crystals produced at various input salt solution concentrations. Thus, the protocol for collecting crystals should include a way to make sure that crystals exit the outlet tubing and concentrate near the center of the collection slide. Once a reproducible collection method is established, there will be enough crystals collected to perform a more detailed analysis of the chemical composition of the crystals (i.e. COM vs COD). The glass slide substrate can be replaced with a suitable substrate (i.e. silicon, BaF₂, ZnSe) for Raman or FTIR analysis of crystal composition.

Another issue that impedes collection results is the tendency for crystals to adhere to the channel. This can be an issue, in general, with crystallization within microfluidic devices. Ideally, for optimal crystal collection and analysis, any crystals formed within the device should flow through the device completely. When crystals stick to the channel walls this could lead to clogged channels and limit experimental run time. In this study, a large section of the crystal line would sometimes break off, thereby disrupting the desired flow profile (Figure 33 a). Because of the design of the devices used in this study, the point at which crystals form in the channel is near the surface of the channel (Figure 34 b). Fabrication of a master structure, that creates a fluid boundary between the PDMS substrate and the point of crystal formation may eliminate this sticking issue (Figure 34 c). Such complex master structures can be made using advanced microfabrication techniques, for example 3-D printing and laser microfabrication.

Throughout this study, there was also consistent variability in the times that a salt line was optically detected in the device. When input salt concentrations are equal the time of line appearance should be the same and reproducible. As mentioned previously (Section 3.A.2.b and Appendix) even though syringe pumps were started in quick succession, it still took time for each syringe pump to engage the syringe (to begin to pump fluid from the syringe). This results in different times in which the different input salts reached the channel. In order to eliminate this issue, the protocol for device operation can be changed to ensure that the salts reach the channel at the same time. This could be accomplished by letting each salt solution flow through the device (after the syringe switch protocol to salt solutions) separately to “prime” the tubing with input salt solutions.

Experimental conditions, such as concentration, can be changed for future experiments. In this study 20, 40 and 60 mM input concentrations were studied. From the results of this study, 20 mM input salt concentrations did not form a line that was visible in the device. It would be constructive to test the equimolar concentrations between 20 mM and 40 mM to determine the lowest concentration where the line can still be detected. Once the collection issue is resolved, it is suspected that there will be a noticeable difference in size and possibly shape of the crystals formed from equimolar input salt concentrations.

It has been reported that a dietary increase in either calcium or oxalate ions can lead to stone formation, therefore future studies should include non-equimolar concentrations of input salts.⁸ For example, 20 mM Ca^{2+} with 40 mM $\text{C}_2\text{O}_4^{2-}$, and vice versa (40 mM $\text{C}_2\text{O}_4^{2-}$ with 20 mM Ca^{2+}). Various combinations of non-equimolar input

salt concentrations (between 20 mM and 60 mM) could be investigated. It is suspected that the non-equimolar input concentrations will impact the; line appearance time, length of line, location of formation in the center channel and shape and size of crystals collected. The results of non-equimolar studies may provide information on which ion favors either COM or COD formation.

Lastly, various other inhibitory additives, such as polyaspartic acid (PolyD) and polyglutamic acid (PolyE), could be tested using the same process as the NaPA (Figure 35). If these other additives are considered inhibitory as well, the results (i.e. line appearance time, and growth) should be similar to the NaPA results. The shape and size of crystals collected with these additives can be compared and further analysis of the exact composition of the crystals can be determined via spectroscopic methods (FTIR, Raman). It would also be interesting to see test results of combined additives. For example, adding NaPA and PolyD to the center stream of the device could lead to an even more drastic change in line growth or crystal shape.

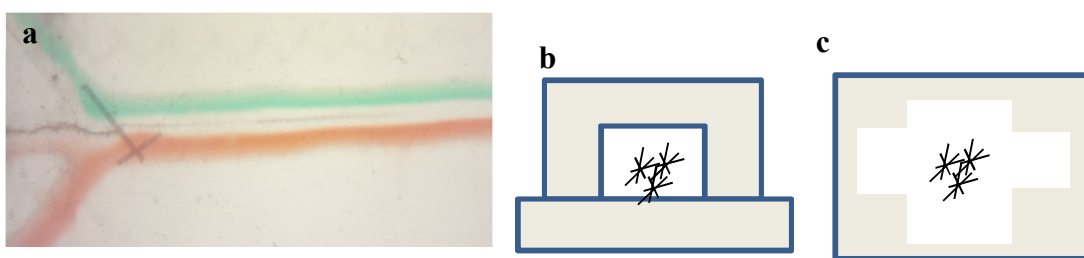


Figure 34. (a) Image of crystal line breaking into pieces. (b) Schematic of cross-section current microchannel design and crystals forming near the surface. (c) Schematic of future microchannel design.

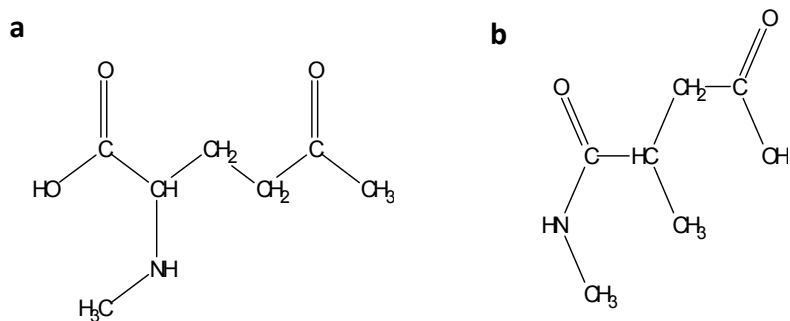


Figure 35. Chemical structures of polyglutamic acid monomer (a) and polyaspartic acid monomer (b).

References

- (1) Scales, C. D.; Smith, A. C.; Hanley, J. M.; Saigal, C. S. *Eur. Urol.* **2012**, 62 (1), 160–165.
- (2) Matlaga, B. R. *Eur. Urol.* **2012**, 62 (1), 166–167.
- (3) Foster, G.; Stocks, C.; Michael, S. *Healthcare Cost and Utilization Project STATISTICAL BRIEF # 139.* **2012**, 56 (3), 1–10.
- (4) Pearle, M. S.; Calhoun, E. A.; Curhan, G. C. *J. Urol.* **2005**, 173 (3), 848–857.
- (5) Raheem, O. A.; Khandwala, Y. S.; Sur, R. L.; Ghani, K. R.; Denstedt, J. D. *Eur. Urol. Focus* **2017**, 3 (1), 18–26.
- (6) Kavanagh, J. P.; Jones, L.; Rao, P. N. *Clin. Sci. (Lond).* **2000**, 98 (2), 151–158.
- (7) Talham, D. R.; Backov, R.; Benitez, I. O.; Sharbaugh, D. M.; Whipps, S.; Khan, S. R.; Uni, V.; Gaines, V. *Langmuir* **2006**, 22 (16), 2450–2456.
- (8) Brzica, H.; Breljak, D.; Burckhardt, B. C.; Burckhardt, G.; Sabolić, I. *Arch. Ind. Hyg. Toxicol.*
- (9) Cerini, C.; Geider, S.; Dussol, B.; Hennequin, C.; Daudon, M.; Veessler, S.; Nitsche, S.; Boistelle, R.; Berthézène, P.; Dupuy, P.; Vazi, A.; Berland, Y.; Dagorn, J. C.; Verdier, J. M. *Kidney Int.* **1999**, 55 (5), 1776–1786.
- (10) Thongboonkerd, V.; Semangoen, T.; Chutipongtanate, S. *Clin. Chim. Acta.* **2006**, 367 (1-2), 120–131.
- (11) Thurgood, L. A.; Wang, T.; Chataway, T. K.; Ryall, R. L. *J. Proteome Res.* **2010**, 9, 4745–4757.
- (12) Prot, J.; Bunescu, A.; Elena-herrmann, B.; Aninat, C.; Choucha, L.; Griscom, L.; Razan, F.; Bois, F. Y.; Legallais, C.; Brochot, C.; Corlu, A.; Emmanuel, M.; Leclerc, E. *Toxicol. Appl. Pharmacol.* **2012**, 259 (3), 270–280.
- (13) Qiu, S. R.; Wierzbicki, A.; Salter, E. A.; Zepeda, S.; Orme, C. A.; Hoyer, J. R.; Nancollas, G. H.; Cody, A. M.; De Yoreo, J. J. *J. Am. Chem. Soc.* **2005**, 127 (25), 9036–9044.
- (14) Sheng, X.; Jung, T.; Wesson, J. A.; Ward, M. D. *Proc. Natl. Acad. Sci. U. S. A.* **2005**, 102 (2), 267–272.
- (15) Hess, B.; Meinhardt, U.; Zipperle, L.; Giovanoli, R.; Jaeger, P. *Urol. Res.* **1995**, 23 (4), 231–238.
- (16) An, Z.; Lee, S.; Oppenheimer, H.; Wesson, J. A.; Ward, M. D. *J. Am. Chem. Soc.* **2010**, 132 (38), 13188–13190.

- (17) Wei, X.; Yang, J.; Li, Z.; Su, Y.; Wang, D. *Colloids Surfaces A Physicochem. Eng. Asp.* **2012**, *401*, 107–115.
- (18) Kulaksizoglu, S.; Sofikerim, M.; Cevik, C. *Int. J. Urol.* **2007**, *14* (3), 214–218.
- (19) Abdel-Aal, E. A.; Daosukho, S.; El-Shall, H. *J. Cryst. Growth* **2009**, *311* (9), 2673–2681.
- (20) Brzica, H.; Breljak, D.; Burckhardt, B. C.; Burckhardt, G.; Sabolić, I. *Arh. Hig. Rada Toksikol.* **2013**, *64* (4), 609–630.
- (21) Wesson, J. A.; Worcester, E. M.; Kleinman, J. G. *J. Urol.* **2000**, *163* (4), 1343–1348.
- (22) Abdel-Aal, E. A.; Daosukho, S.; El-Shall, H. *J. Cryst. Growth* **2009**, *311* (9), 2673–2681.
- (23) Farmanesh, S.; Chung, J.; Chandra, D.; Sosa, R. D.; Karande, P.; Rimer, J. D. *Journal of Crystal Growth*. **2013**, 373, 13–19.
- (24) Whitesides, G. M. *Nature* **2006**, *442*, 368–373.
- (25) Mark, D.; Haeberle, S.; Roth, G.; Von Stetten, F.; Zengerle, R. *Chem. Soc. Rev.* **2010**, *39* (3), 1153–1182.
- (26) Dittrich, P. S.; Manz, A. *Nat. Rev. Drug Discov.* **2006**, *5* (3), 210–218.
- (27) Fiorini, G. S.; Chiu, D. T. *Biotechniques* **2005**, *38* (3), 429–446.
- (28) Van den Berg, A.; Bergveld, P. *Lab Chip* **2006**, *6* (10), 1266–1273.
- (29) Hitzbleck, M.; Delamarche, E. *Chem. Soc. Rev.* **2013**, *42*, 8494–8516.
- (30) Hansen, C.; Quake, S. R. *Current Opinion in Structural Biology*. 2003, pp 538–544.
- (31) Weibel, D. B.; Whitesides, G. M. *Current Opinion in Chemical Biology*. 2006, pp 584–591.
- (32) Yashina, A.; Meldrum, F.; Demello, A. *Biomicrofluidics* **2012**, *6* (2), 1–10.
- (33) Yin, H.; Bozhi, J.; Dobson, P. S.; Mosbahi, K.; Glidle, A.; Gadegaard, N.; Freer, A.; Cooper, J. M.; Cusack, M. *Anal. Chem.* **2009**, *81* (1), 473–478.
- (34) Leng, J.; Salmon, J.-B. *Lab Chip* **2009**, *9* (1), 24–34.
- (35) Jo, H.; Blum, F. D. *Langmuir* **1999**, *15* (7), 2444–2449.
- (36) Xia, Y.; Whitesides, G. M. *Angewandte Chemie (International Ed.)* **1998**, *37*, 550.

- (37) Wang, Y.; Lee, D.; Zhang, L.; Jeon, H.; Mendoza-Elias, J. E.; Harvat, T. A. ; Hassan, S. Z.; Zhou, A.; Eddington, D. T.; Oberholzer, J. *Biomed. Microdevices* **2013**, *14* (2), 419–426.
- (38) Jung, T.; Kim, W.-S.; Kyun Choi, C. *J. Cryst. Growth* **2005**, *279* (1-2), 154–162.
- (39) Jung, T.; Kim, W.-S.; Choi, C. K. *Mater. Sci. Eng. C* **2004**, *24* (1-2), 31–33.

Appendix

A. Master structure fabrication

The PDMS molds were not curing completely at the interface of the PDMS and the master structure. It was possible that there could be excess photoinitiator in the master structure affecting the cross-linking process of the PDMS. To test this hypothesis, a drop of photoinitiator was placed onto a fluorocarbon-coated glass slide, PDMS was poured over the photoinitiator and was heated for ~30 minutes at 110°C. This temperature was chosen to facilitate fast PDMS curing. The results of this test proved that the TPOL was in fact limiting the curing of the PDMS. Several tests were completed to find the time and temperature necessary for the TPOL to not interfere with PDMS cross-linking and avoid the master structure cracking.

B. Pump start up traits

The syringe pumps were stopped when the syringes were being switched to salt solutions (section 2.C.1 describes syringe switch protocol). If the syringe switch was performed while the pumps were running, the laminar flow profile was disturbed. The syringe pumps were started sequentially (i.e., middle stream, side-stream, side-stream) as quickly as possible. Even though the syringe pump starts were quick, it still took time for the syringe pump to engage with the syringe and get both side streams to flow at the same time. This issue resulted in variability in the time it took for the salt concentrations to flow completely through the tubing to the microchannel.